Clean Energy Science and Technology 2024, 2(3), 176.
https://doi.org/10.18686/cest.v2i3.176

Review

Recent advances in sustainable nanomaterials for energy conversion and environmental remediation via photocatalysis

Muhammad Shoaib Khalid[1,4], Gao Li[1,2,4,*], Tasmia Azam[1,4], Muhammad Asad[3], Zhen Zhao[2,*]

[1] State Key Laboratory of Catalysis, Dalian Institute of Chemical Physics, Chinese Academy of Sciences, Dalian 116023, Liaoning Province, China
[2] Institute of Catalysis for Energy and Environment, College of Chemistry and Chemical Engineering, Shenyang Normal University, Shenyang 110034, Liaoning Province, China
[3] School of Materials Science and Engineering, Henan University of Technology, Zhengzhou 450001, Henan Province, China
[4] University of Chinese Academy of Sciences, Beijing 100049, China
*** Corresponding authors:** Gao Li, gaoli@dicp.ac.cn; Zhen Zhao, zhenzhao@cup.edu.cn

CITATION

Khalid MS, Li G, Azam T, et al. Recent advances in sustainable nanomaterials for energy conversion and environmental remediation via photocatalysis. Clean Energy Science and Technology. 2024; 2(3): 176. https://doi.org/10.18686/cest.v2i3.176

ARTICLE INFO

Received: 13 May 2024
Accepted: 19 July 2024
Available online: 25 September 2024

Abstract: Photocatalysis is of particular interest because it can be utilized for reducing air pollution and decreasing greenhouse gas emissions. This review examined the latest advances in layered photocatalytic nanomaterials and single-atom catalysts and discloses the synthesis, structural features, and ways to enhance their catalytic ability. In particular, we describe the peculiarities of catalysis mechanisms in CO_2 conversion, pollutant and NO_x removal, and nitrogen reduction. The current trends in this field and the potential areas for further research are also discussed in this review. It is important to emphasize that single-atom catalysts possess distinct advantages to substantially improve the efficiency of energy conversion processes. The materials related to the synthesizing and post-processing of layered semiconductor catalysts and single-atom catalysts can be useful for other researchers and stakeholders.

Keywords: photocatalysts; perovskite oxides; single-atom catalysts; heterojunctions

1. Introduction

In the past few centuries, there has been a growing concern regarding the gradual depletion of abundant fossil fuel reserves beneath the earth's crust. The rapid growth of the global population has exacerbated this issue, making it increasingly challenging to meet the planet's energy demands. The increasing demand for fossil fuel leads to high levels of dangerously toxic gasses, such as CO_2 and CO. Environmental deterioration and climate change have resulted from such gases [1–3]. Moreover, the massive burning of fossil fuels has been a key figure contributing to the greenhouse effect, threatening the ecosystem by raising levels of CO_2 in the atmosphere dramatically [4]. The combustion of fossil fuels in the industry has been one of the key factors in soaring concentration of CO_2 in the atmosphere. Based on predictions, due to the greenhouse effect, CO_2 accumulating over time has the potential to reach 750 ppm from its present level of 400 ppm (which is also 0.04%) [5]. This could in turn mean temperature rising by 5–9 °C and rainfall decreasing or increasing worldwide. Considering this reality, there is an urgent need to promote the development and use of renewable energy sources [4–6]. This will not only meet the needs of society but also be beneficial in resisting global warming's effects on society. Air pollutants consist of complex blends of harmful chemicals. They include gases and other substances. Their concentrations and residence times in the

atmosphere are large enough to bring adverse environmental repercussions and ecotoxicological effects. For example, NO_x, mainly nitrogen dioxide (NO_2) and nitrogen monoxide (NO), is one of the most widespread of several other pollutants found in nature, resulting in air pollution. The free radicals of NO_x can merge with other atmospheric ingredients to produce smog and acid rain, which causes health concerns, including multiple diseases (e.g., eye and throat irritation) and increased susceptibility to respiratory infections. Additionally, NO_x emissions contribute indirectly to stratospheric ozone depletion and also have a greater effect on greenhouse gas emissions and global warming [7,8]. Conversely, for terrestrial life, reactive fixed nitrogen exists only in small concentrations. It must be changed into fixed nitrogen with no N≡N bonds and into significant products, including NH_3, nitrates, and $CO(NH_2)_2$, which living organisms can assimilate instead [9,10]. As the cornerstone of the global nitrogen cycle, turning atmospheric NO_x into fixed nitrogen and inverse alteration to maintain the nitrogen cycle in balance are among the chief biogeochemical processes on the earth. The earth has seen natural nitrogen-fixing processes for almost 2 billion years, with an estimated annual fixation rate of about 150 to 200 Tg [11]. One of the promising alternative fuel sources is ammonia (NH_3), with a substantial hydrogen concentration of 17.6 wt%. The major part of the compound is derived from nitrogen fixation processes [12]. Apart from the fact that this compound might be a good solution for the transportation sector at short notice, it is also a great long-term solution, since it has zero carbon emissions [13].

Currently, various innovative catalytic techniques, including electrocatalysis and photocatalysis, are being developed to investigate the nitrogen-fixation capabilities of catalysts [14]. Photocatalytic nitrogen fixation is regarded as one of the most promising alternatives due to its utilization of abundant solar energy for nitrogen fixation reactions. These reactions include the nitrogen reduction reaction and the nitrogen oxidation reaction under favorable conditions. In 1977, Schrauzer and Guth found that nitrogen (N_2) can be photocatalytically reduced to ammonia (NH_3) and hydrazine (N_2H_4) over TiO_2 and that the inclusion of Fe_2O_3 boosts the nitrogen-fixation efficiency of TiO_2 [15]. Since then, various approaches, such as inducing manufacturing defects, employing supporting co-catalysts, and creating heterojunctions, have been devised to enhance the efficiency of nitrogen-fixation processes [16].

Photocatalysis has demonstrated great promise as a green technology since 1980 due to its inherent economic and sustainable energy advantages over other approaches, but certain fundamentals require further progress to unlock its full potential [17,18]. The initial breakthroughs in harnessing photocatalysis for environmental remediation and CO_2 reduction opened new possibilities for sustainably treating air pollutants. However, conventional metal oxide semiconductors utilized until now have been constrained by insufficient conversion of sunlight to usable forms of energy and difficulty scaling up from the laboratory to the commercial scale [19].

Researchers have attempted to solve bandgap engineering challenges using photocatalysts that are more energy-efficient [20,21]. In addition to these technologies, the promising approaches of single-atom catalysts and layered semiconductor nanomaterials have received considerable attention. For a

heterogeneous catalytic process in the chemical industry to function effectively, the reaction should occur at the interface where the solid catalyst interacts with the active sites of reactants [22]. Thus, one of the simplest and most widely used techniques to gain such properties is reducing the size of catalyst particles to the nanometer range. The physical and chemical properties of these advanced catalysts are due to their high surface area-to-volume ratio [23,24]. This breakthrough gives new ways in photocatalysis to study photo-responsive materials and their mechanisms in both pollutant degradation and CO_2 photoreduction. Among them, layered photocatalysts, which possess a large interface area and exhibit enhanced performance properties owing to their unique layered structure, have been studied. Three key characteristics are shared among these novel photocatalysts for environmental cleaning. Layered or stacked 2D nanomaterials have been studied due to their ordered morphologies, tunable CO_2 adsorption per unit volume, and easy adjustment of the range of anions or cations [25].

Moving forward, sustained research is imperative to enhancing photocatalytic efficiency and viability at an industrial scale through novel materials, structures, or methods so that this technology may fully realize its promising early applications and become transformative. Semiconductor photocatalysis is one of the emerging novel sustainable energy approaches in recent years [26]. This technique is capable of not only converting solar energy into utilizable fuels that can be stored, transferred, and utilized but also supporting waste reduction and pollutant decomposition [27]. Overall, the photocatalytic process comprises three basic stages: 1) light absorption, 2) charge separation and migration, and 3) surface redox reactions of pollutants [28]. The result of this process may greatly depend upon many factors, among which are the optical properties, size, surface area, and morphology of the semiconductor photocatalysts [29]. In addition, the energy of the bandgap may define the range of light absorption, while the position of the valance and conduction band edges may establish redox potentials.

There are many reviews discussing the synthesis methods, structural properties, and applications of layered photocatalytic nanomaterials and single-atom catalysts in diverse fields [30–34]. The present review reveals an unbiased perspective regarding the concrete progress in the context of perovskites and single-atom catalysts in CO_2 reduction and nitrogen fixation. In particular, recent studies on current challenges, with a focus on general strategies, synthesis methods, and structural properties, are discussed. Also, the catalytic functions of these materials are elaborated, with primary realization of such critical processes as CO_2 into valuable fuels and environmental applications involving NO_x and nitrogen reduction. In the conclusion, potential development trends in the field of layered and single-atom catalysts are outlined. This review presents a comprehensive summary of the synthesis, modification, and applications of both layered semiconductor catalysts and single-atom catalysts. A significant aspect of the review is the insight into the mechanisms behind the modulation of the electronic structure and the coordination environment of single-atom catalysts to affect catalytic activity, stability, and selectivity. The conclusion lists the most significant factors or trends, accompanied by the highest potential, challenges, and opportunities for single-atom catalysts in the domain of energy conversion.

2. Advances in metal-based layered photocatalytic nanomaterials

Metal-infused layered photocatalytic nanomaterials are a unique type of photocatalytic materials, which are of special interest for energy conversion and environment remediation. They can be classified into several types, among which are layered perovskite oxides, layered double hydroxides (LDHs), and transition metal dichalcogenides. Since all these materials have different structural and chemical properties, they may serve as a basis for developing other environment-friendly methodologies.

2.1. Multi-layered perovskite oxides

The term "perovskite" was coined by German scientist Gustav Rose in 1839 upon his identification of the crystalline structure of $CaTiO_3$, which he named in tribute to Russian mineralogist Count Lev Aleksevich von Perovski [35]. Over several decades, inexpensive perovskite oxides, described by the typical formula of ABO_3 (**Figure 1(a)**), have grown tremendously reputable as an economically practical and earth-abundant category of multifunctional materials [36]. In an ideal cubic-symmetry form, the larger A-site cation is frequently a rare-earth or alkaline earth metal, exhibiting extensive 12-cornered coordination with oxygen atoms, whereas the smaller B-site cation commonly is a transition metal demonstrating compressed six-fold coordination with oxygen [37]. Currently, multiple perovskite oxide semiconductor nanomaterials have been discovered, including periodic table elements which can be either A or B sites in the lattice structure (**Figure 1(b)**) [38]. Notably, perovskite oxides offer an advantageous property above other non-precious metal oxides owing to their intrinsic capacity for compositional and structural adaptability. There are several ways in which the architecture may be opened. One is a stack consisting of alternating layers of perovskite slabs with weak electrostatic interactions between them [39]. Based on how the stacked layers orient in space relative to the cubic perovskite axis, we generally divide layered perovskite structures into three types: (110), (100), and (111) [31]. The formulations of the first two perovskite structures are ($A_{n+1}B_nO_{3n+3}$) and ($A_nB_nO_{3n+2}$), respectively, where the values of *n* are determined by comparing the formulaic composition of these two types with structural details, such as the stacking sequence. The (100) perovskite structures have several formulations: (Bi_2O_2) ($A_{n-1}B_nO_{3n+1}$) in its Aurivillius phase, $A_{n+1}B_nO_{3n+1}$ or $A'_2A_{n-1}B_nO_{3n+1}$ in its Ruddlesden-Popper phase, and $A'[A_{n-1}B_nO_{3n+1}]$ in its Dion-Jacobson phase, where the number of BO_6 octahedra in each layer is denoted as "*n*" (**Figure 1(c)**) [34].

A bandgap value is significant in the context of the photocatalytic phenomenon, since it determines the energy for electron excitation from the valance band to the conduction band. The bandgap energies and band edges of perovskite can be modified by changing the composition of both sites A and B (**Figure 1(d)**) [38]. A distinguishing characteristic of photocatalysis lies in the diverse chemical composition and structural architecture exhibited by perovskite oxides. Bi_2MoO_6 synthesized by Li et al. [40] is a type of Aurivillius-phase ferroelectric compound, which has attracted the interest of many researchers. By combining the CTAB-assisted hydrothermal method and corona polling post-treatment, the authors

produced ultrathin Bi_2MoO_6 nanosheets with strong ferroelectric features (**Figure 1(e)**). The nanosheets greatly overcame the charge recombination between layers and also enhanced the charge separation, as well as CO_2 absorption on Bi_2MoO_6. Such boost in catalytic sites and the enhancement of the internal electric field had a synergistic effect that boosted the photocatalytic activity for CO_2 reduction, resulting in a considerable CO evolution rate of 14.38 $\mu mol \cdot g^{-1} \cdot h^{-1}$ achieved for polarized Bi_2MoO_6 ultrathin nanosheets in a gas-solid system (**Figure 1(f)**). On the other hand, Yu et al. [41] synthesized ferroelectric $SrBi_2Nb_2O_9$ nanosheets via the one-pot hydrothermal synthesis route. Photogenerated electrons transferred to NbO_6 octahedron layers and migrated along the c-axis, while the holes were mainly confined in the *ab*-plane of Bi_2O_2 layers (**Figure 1(g)**). This facilitated anisotropic transport for increased charge transfer. Interestingly, when the two synthesized annealed samples were compared, the formation of both CH_4 and CO gave greater efficiency as compared with non-annealed $SrBi_2Nb_2O_9$ as the catalyst for the CO_2 photoreduction process (**Figure 1(h)**).

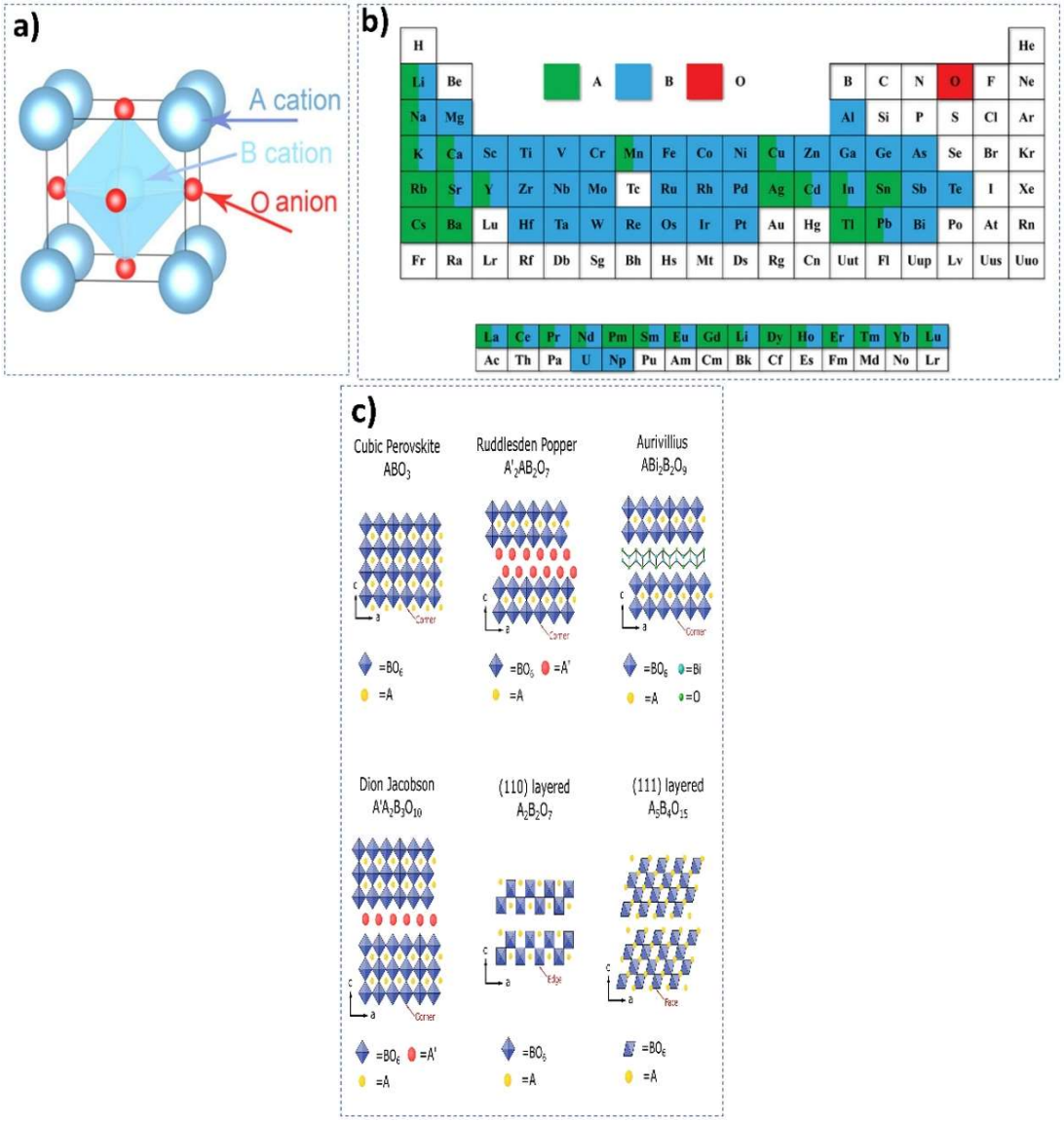

Figure 1. (*Continued*).

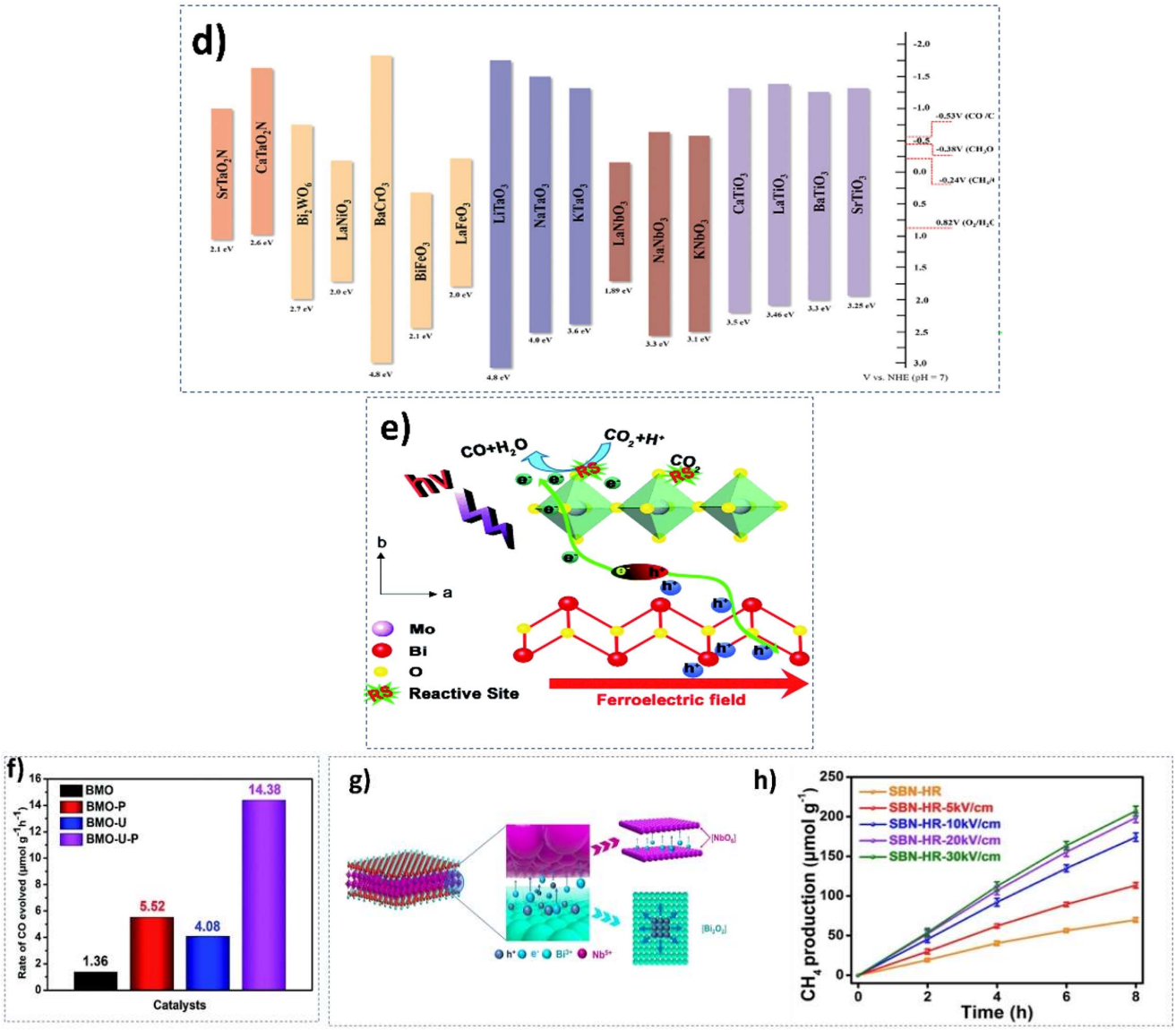

Figure 1. (a) Crystal lattice of ABO_3 perovskite oxide [36]. **(b)** Multiple elements of A and B sites [38]. **(c)** Cubic and layered arrangements of perovskites [34]. **(d)** Band structure and redox potentials of perovskite oxides and oxynitrides [38]. **(e)** Charge separation mechanism and CO_2 reduction in ultra-thin Bi_2MoO_6. **(f)** CO production rate of ferroelectric thin layer of Bi_2MoO_6 [40]. **(g)** Schematic representation of charge (e^- and h^+) separation and migration within unit. **(h)** Production curves for CH_4 over polarized $SrBi_2Nb_2O_9$ [41].

For the alignment of stacked layers in perovskite oxides relative to the ideal ABO_3 structure axis, other layered arrangements of the (100) type include the Ruddlesden-Popper phase structure (**Figure 2(a)**), and the Dion-Jacobson phase structure (**Figure 2(b)**), where the chemical compositions are described by the general formulas $A'_2A_{n-1}B_nO_{3n+1}$ and $A'[A_{n-1}B_nO_{3n+1}]$, respectively [42]. Both categories of perovskite oxides are of considerable interest for their potential applications in H_2 production. Particularly notable among the Ruddlesden-Popper type is $H_{1.81}Sr_{0.81}Bi_{0.19}Ta_2O$, which was found to have a H_2 production rate of 57670 $\mu mol \cdot g^{-1} \cdot h^{-1}$ in the presence of 4.76% methanol [43]. Sr_2TiO_4 and La_2NiO_4 showcase 2D perovskite crystals with layered structures and are perfect examples of the Ruddlesden-Popper type, exhibiting pronounced photocatalytic activity in the

degradation of environmental pollutants under photon exposure. By using a sonochemical technique, they synthesized Sr_2TiO_4 nano-assemblies and applied them for the degradation of dyes under ultraviolet irradiation and achieved 76% degradation of dyes, and also they studied how the photocatalyst's layered morphology and arranged crystalline order contributed to its photocatalytic activity through efficient charge migration and pollutant adsorption, see **Figure 2(c)** [44]. In another study, a novel La_2NiO_4 morphology with a hollow sphere architecture was synthesized via a facile hydrothermal method using glycerol. It exhibited exceptional activity as a photocatalyst for organic contaminant phenol and anionic dyes, degrading as much as 87% under light irradiation under a dark condition over 12 h [45]. The proposed mechanism of the catalytic reactions using aggregated La_2NiO_4 nanoplates and HS-La_2NiO_4 can be seen in **Figure 2(d)**. Dion-Jacobson Monovalent alkali cation A′ between perovskite-like crystals was evident in the crystal structure of Dion-Jacobson phases, such as $RbLnTa_2O_7$ [46] and KCa_2Nb_3O10 [47]. It has been observed that $Ca_2Ta_3O_{9.7}N_{0.2}$ nanosheets derived from Dion-Jacobson-phase layered perovskite oxynitride $CsCa_2Ta_3O_{9.7}N_{0.2}$ by proton exchange and a two-step process of intercalation by ethylamine and tetrabutylammonium ions showed photocatalytic activity concerning hydrogen evolution under excitation with visible light. The TEM images, SAED pattern, and HAADF-STEM images are shown in **Figure 2(e)**. Performance curves for hydrogen evolution reaction from water splitting of the nanosheets under visible light illumination are shown in **Figure 2(f)** [48].

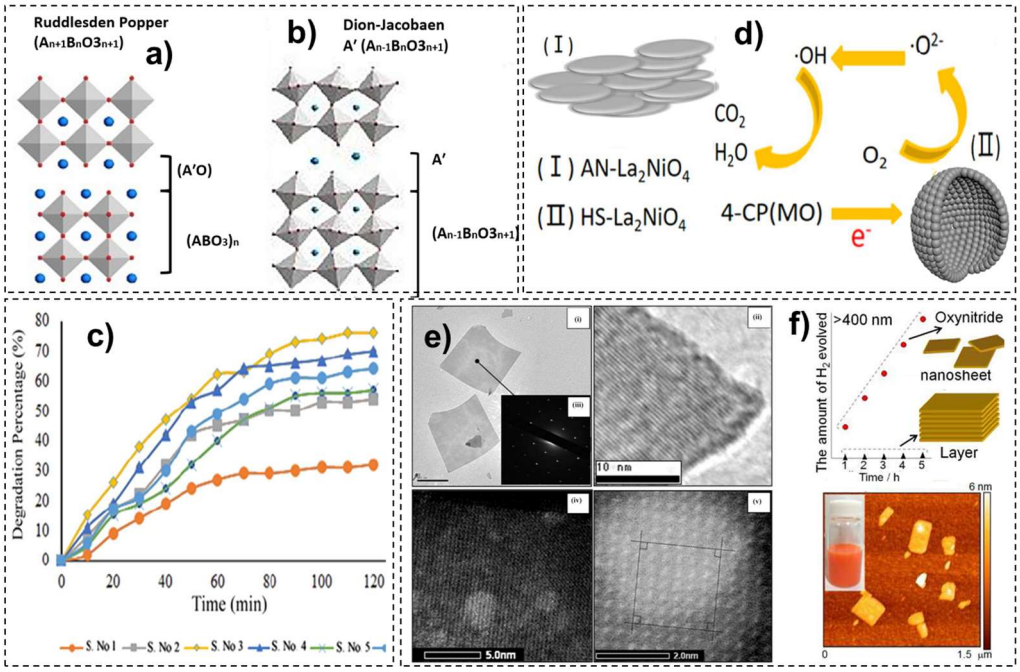

Figure 2. (a) Ruddlesden-Popper phase structure of layered perovskite oxides [49]. **(b)** Dion-Jacobson phase structure of perovskite oxide [19]. **(c)** Performance curves for degradation of methyl orange by using Sr_2TiO_4 samples [44]. **(d)** Schematic illustration of catalytic process of AN-La_2NiO_4 and HS-La_2NiO_4 [45]. **(e)** (i, ii) TEM images of oxynitride nanosheets of $Ca_2Ta_3O_{10-x}N_y$, (iii) SAED pattern of $Ca_2Ta_3O_{10-x}N_y$ nanosheets, and (iv, v) HAADF-STEM images of $Ca_2Ta_3O_{10-x}N_y$ nanosheets. **(f)** Performance curves for hydrogen evolution of oxynitride nanosheets and AFM images of $Ca_2Ta_3O_{10-x}N_y$ nanosheets [48].

2.2. Synthesis of layered perovskite oxides

Perovskite oxides have been synthesized through numerous experimental techniques employed by researchers, including the sol-gel method, chemical precipitation, simple hydrothermal synthesis, combustion synthesis, and solid-state reaction method [50–52]. Significant concerns center on stability, efficiency, and improved crystal structure involving a low magnitude of defects. The synthesis is also essential for achieving beneficial outcomes when conducted at ambient conditions, as it enhances the high crystallinity of perovskite oxides, thereby considerably reducing the energy employed in the synthesis [53]. Such techniques must be analyzed and understood, as they influence the physical and optical properties of the resultant material. The high performance of these materials is typically dependent on various factors, including surface area and bandgap. Generally, a high surface area enhances the number of reaction sites and adsorption of a photocatalyst. Moreover, an optimal bandgap permits the absorption of a definite wavelength of light. Therefore, different types of synthesis techniques for perovskite materials have been employed to improve their properties. In this section, we summarized a few synthesis techniques that are generally used.

2.2.1. Sol-gel method

The sol-gel process is an easy approach for synthesizing oxide materials through inorganic polymerization of molecular precursors. Recently, the sol-gel method has been widely used for the synthesis of perovskite-type complex oxides. Compared with the traditional solid-state reaction method, it offers high phase purity, precise compositional control, and reduced synthesis temperatures. In a typical sol-gel process, metal precursors, such as metal nitrates and acetates, are dissolved and mixed in precise stoichiometric ratios to create a clear solution. Chelating agents, such as citric acid and ethylenediaminetetraacetic acid, are then added. Sometimes, binding agents, such as ethylene glycol, are included as well. The molar ratios of the metal precursors, chelating agents, and optional binding agents are meticulously adjusted to achieve optimal conditions. To ensure thorough chelation, the pH of the solution is carefully regulated within a specific range (typically 6–8) using aqueous ammonium hydroxide. Following mixing, the solution undergoes stirring and evaporation under controlled conditions near 100 ℃, resulting in the formation of a gel. This gel is subsequently subjected to heating at approximately 300 ℃ to induce the formation of a porous material. Further calcination at elevated temperatures and under defined atmospheres completes the transformation into the final product. It is noteworthy that these procedural details may vary depending on the specific composition of the targeted perovskite material.

Parida et al. [54] reported the synthesis of nanocrystals of $LaFeO_3$ via the sol-gel method. The precursors of $LaFeO_3$ and citric acid were blended to obtain a stable nitrate-citrate sol, which was dried for abandoning the solvent at 130 ℃. During the thermal treatment, the sol changed in color and viscosity. The brown-colored porous dry gel was spontaneously burnt by further heating due to the thermally induced redox reaction. For the synthesis of $ZnTiO_3$ using the sol-gel method, $Zn(CH_3COO)_2{\cdot}2H_2O$ and tetrabutyl titanate were utilized as precursors, with benzene-1,3,5-tricarboxylic acid introduced as a novel chelating agent It is essential

to note the significant impact of the chelating agent on the product's morphology, size, and purity characteristics [55]. The molar ratio of the chelating agent to tetrabutyl titanate remained constant, which was 3:1. A schematic illustration of the formation of $ZnTiO_3$ nanoparticles can be seen in **Figure 3(a)**. Limitations of the sol-gel technique include defects from the drying, such as shrinks, residual pores, or cracking. Also, this method is generally costly and its industrial applications face difficulties, which limits its application at a large scale. Tetra (n-butyl) ammonium hydroxide can be employed as an intercalation agent to realize the facile exfoliation of bulk-layered perovskite oxides into ultra-thin nanosheets, which possess a large specific surface area and plenty of reaction sites [56]. The 2D structure of the layered perovskite oxides has special structural properties, which can achieve an efficient anisotropic charge transfer. The synthesis of layered perovskite oxide Sr_2TiO_4 was carried out using the sol-gel method [57]. Strontium nitrate and titanium isopropoxide served as the precursor materials, in addition to the use of nitric acid to avoid the hydrolysis effect. The complexing agent used in the synthesis was citric acid monohydrate, which was employed throughout the process until the formation of a homogeneous solution. After the exfoliation of the product in a H_2-rich environment, a white powder of H-Sr_2TiO_4 was obtained, as shown in **Figure 3**(**b)**. Due to its narrow bandgap and reduced electron recombination, it is a dependable catalyst for CO_2 photoreduction reactions.

2.2.2. Hydrothermal method

Hydrothermal synthesis is regarded as the most prospective among all alternative methods due to its increased capacity to prepare numerous materials, particularly various molecular sieves and two-layer and three-layer compounds. It is a wet chemical technology that is particularly promising because of its ability to obtain highly crystalline products that are usually uniform and possess little aggregation. The morphology and crystalline architecture of the resultant products highly depend on the reaction conditions of the hydrothermal method [58]. Kalaiselvi et al. [59] successfully synthesized $LiTaO_3$ by using the simple hydrothermal approach, as shown in **Figure 3(c)**, and also investigated the characteristic physical properties of the photocatalytic hydrogen evolution, as shown in **Figure 3(d)**. Ag-doped $LiTaO_3$ gave a high yield of 240 $\mu mol \cdot g^{-1} \cdot h^{-1}$ as compared with that of N-doped $LiTaO_3$. Dawi et al. [60] identified novel octahedral carbonized perovskite nanomaterials F-doped $NiTiO_3$. Synthesis was performed through the hydrothermal route to promote heterogeneous gas-phase CO_2 reduction to CH_4. The study used equimolar amounts of Ni and Ti precursors dissolved in an ethylene glycol solution. In the next step, diluted HNO_3 solution and H_2O_2 solution were added dropwise under continuous stirring. The resultant mixture was transferred into a stainless-steel autoclave at 150 °C for 18 h. The authors concluded that the catalytic methane production rate of F-doped $NiTiO_3$/C was slightly higher, i.e., 1.6 times that of pristine $NiTiO_3$/C. Even after five successive cycles, a nearly constant performance was shown by the catalytic activity. The amount of the F-dopant had a noticeable effect on the CO_2 photoreduction rate, with the highest activity observed at a NaF content of 0.04 $mol \cdot L^{-1}$. F kinetically boosted the electroactive surface area

and altered the charge transfer process, increasing the steps through which CO reduction occurred, as shown in **Figure 3(e)**.

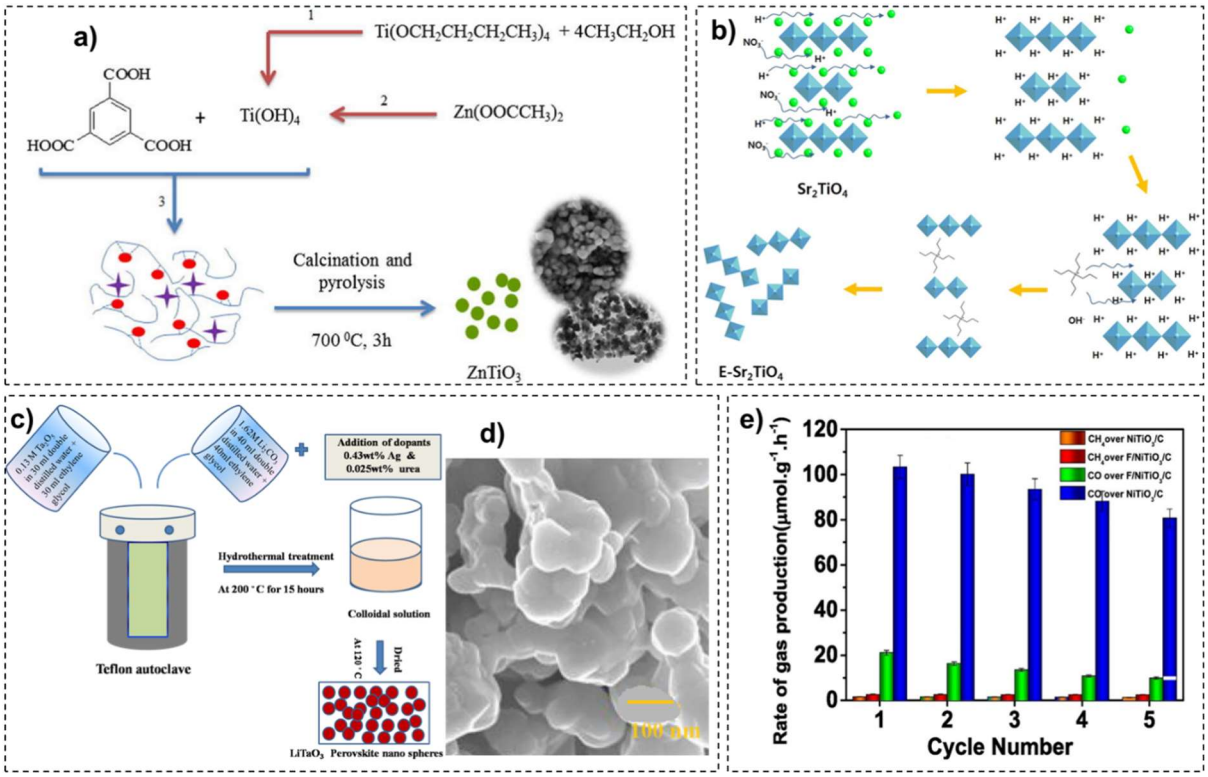

Figure 3. (a) Schematic representation of synthesis process of $ZnTiO_3$ nanoparticles using sol-gel method [55]. **(b)** Steps of synthesis of Sr_2TiO_4 and exfoliated forms E-Sr_2TiO_4 and H-Sr_2TiO_4 [57]. **(c)** Schematic view of experimental setup for synthesizing $LiTaO_3$ nanoparticles [59]. **(d)** FESEM images of pristine $LiTaO_3$ [59]. **(e)** Recycling test after five cycles of as-prepared photocatalysts [60].

2.2.3. Solid-state reaction method

The synthesis of perovskite oxides represents an example of the widely employed solid-state reaction method in the field. This technique requires the mixing of metal oxides and metal carbides. Subsequently, the mixture undergoes heating at high temperatures to produce perovskite materials. The calcination temperature is important in the synthesis process. Control over the temperature is critical because the calcination process requires a specific extent. Specifically, excessive temperature may result in sintering, but inadequate temperature does not facilitate the formation of the necessary morphological patterns [61,62]. At present, the landscape of the synthesis method is characterized by some of the method's limitations, with evaluations simplified and complex and expensive methods excluded. The limitations are the high cost of reagents, the demand for sophisticated equipment, the duration of high-temperature processing, and subsequent post-processing and thermal treatment steps. As such, the above factors prevent comprehensive evaluations and applications of the method. To overcome the challenges experienced during the formation of perovskite oxides. Amdouni et al. [63] reported an alternative way to fabricate perovskite oxides by using facile chemical bath synthesis at a low temperature of 50 ℃ and extending it using a single-step annealing treatment. A low-temperature annealing strategy can help to solve the high energy

consumption [64]. The synthesis of $LaFeO_3$ nanoparticles was carried out through the use of the chemical bath approach, where a precursor ratio of 1:1 in volume was used with a solution consisting of 5 mmol of $Fe(NO_3)_3.9H_2O$ and 5 mmol of hydrated rare-earth nitrate salt. The nitrates were dissolved in deionized water, after which an NH_3 solution was used for complexation while stirring. The next step involved heating the solution in an oil bath at 50 ℃ for 2 h. Following filtration, the resultant precipitate was poured out, washed, and annealed at 900 ℃ for 2 h. Solid state reaction method was utilized to synthesize La_2NiO_4. Precursors were accurately weighted in stoichiometric amounts and then combined inside a zirconia media ball mill, where during the milling, ethanol was employed as a dispersant. After 6 h, the powdered mixture was removed and annealed at 1000 ℃ for 8 h with a ramp rate of 10 ℃·min^{-1} to obtain the final product [65].

2.2.4. Diverse synthesis methods

In addition to the previously discussed synthesis techniques, ball milling is an efficient physical method to decrease the particle size of traditionally synthesized perovskites to the sub-micrometer or nanometer scale [66]. However, this technique is characterized by high energy consumption and frequently results in perovskite nanomaterials with non-uniform morphologies, impurities, or amorphous phases. Additionally, alternative synthesis methods have been successfully employed by researchers to fabricate perovskite nanostructures, including combustion synthesis [67], flame spray synthesis [68], microwave-assisted method [69], and coating [70]. For instance, Liu et al. [71] utilized a one-step combustion synthesis to create a nanohybrid of layered perovskite and metal oxide, namely NiO–$(La_{0.613}Ca_{0.387})_2NiO_{3.562}$. Yang et al. [70] developed a hierarchical, porous, and flexible structure consisting of graphene and mesoporous $La_{0.8}Sr_{0.2}MnO_3$ nanosheets arranged in a sandwich-like configuration.

Methods such as sol-gel processing and precipitation are commonly employed to synthesize nanoparticulate perovskites. For the fabrication of perovskite nanofilms, the solid-state reaction method is particularly effective. Methods such as hydrothermal synthesis, template-assisted synthesis, and electrospinning are advantageous for producing nanostructured perovskites with specific morphologies and desirable porosity. **Table 1** summarizes the applications of nanostructured perovskite photocatalysts. Notably, the solid-state reaction method is a widely adopted method for creating perovskite nanostructures.

Table 1. Summary of different perovskite oxides developed via various synthesis routes.

Method	Perovskite	BET surface area	Application	Ref.
Sol-gel	$BaTiO_{3-x}$	24.7 $m^2 \cdot g^{-1}$	OER/ORR	[72]
Sol-gel	$CaMnO_3$	32 $m^2 \cdot g^{-1}$	Li-air batteries	[73]
Precipitation	$La_{0.5}Sr_{0.5}CoO_{2.91}$	11.87 $m^2 \cdot g^{-1}$	Li-air batteries	[74]
Precipitation	$La_{0.8}Sr_{0.2}CoO_{3-\delta}$	4.5 $m^2 \cdot g^{-1}$	OER	[75]
Sol-gel	$LaFeO_3$	25.8 $m^2 \cdot g^{-1}$	OER	[54]
Sol-gel	$ZnTiO_3$	N/A	OER	[55]
Sol-gel	Sr_2TiO_4	1.19 $m^2 \cdot g^{-1}$	CO_2 reduction	[57]
Hydrothermal	$LiTaO_3$	N/A	H_2 evolution	[59]
Solid-state reaction	La_2NiO_4	1.93 $m^2 \cdot g^{-1}$	CH_4 conversion	[65]

2.3. Harnessing potential of perovskite oxides: Innovations in energy solutions and environmental sustainability

A host of semiconductor photocatalysts present challenges of low light absorbance and photogenerated charge carrier recombination, hence their inability to deliver outstanding performance [76]. Most perovskite oxides are attributed with wide bandgaps and will only absorb UV radiation; however, a high percentage of solar radiation comprises visible and near-infrared regions. Therefore, developing photocatalytic materials that can effectively harness visible and near-infrared photon energies is critical. Perovskite-oxide-based photocatalysts are emerging as a substantial interest among scholars regarding routes to the enhanced photocatalytic reduction of CO_2 to provide valuable chemicals. Several strategies have been used to improve the photocatalytic capabilities of perovskite-oxide-based and oxide-based photocatalysts. The bandgap is a crucial parameter in photocatalytic processes, which is determined as the minimum energy required for electron transfer from the valence band to the conduction band. This property and the edge position of the valence band and the conduction band can be controlled by modifying A-site and B-site cations in perovskite oxides [38]. The crystal lattice has three distinct sites, which are A, B, and O, where perovskite oxides' bandgap can be readily altered via heteroatomic doping. The change in the bandgap has been shown to improve the absorbance of the light and enhance photocatalytic efficiency. Nevertheless, one of the most serious issues with present photocatalysts is the recombination of charge carriers upon their formation. Many modification strategies have been utilized based on the core principle of photocatalysis from perovskites, which rely on the chemical composition and crystal structure of perovskites. The formation of Z-scheme heterojunctions [77], doping of cation species [78], and anion doping [79] have been recognized as the most effective strategies to expand photo-absorption into the visible light region for perovskite oxides. Here, we briefly discuss these modern strategies.

2.3.1. Evolving perovskite heterojunction configurations

Photocatalytic materials are substances capable of converting sunlight energy into charged material. This conversion occurs when specific wavelengths of light are absorbed, triggering the generation of charges that migrate from the interior to the surface of the photocatalyst. Once on the surface, these charges react with adsorbed species, leading to reduction and oxidation reactions. Since both electrons and holes are necessary for surface redox reactions, any reactions occurring in the presence of both are deemed to be surface-mediated. In the absence of an imposed potential gradient, the movement of photogenerated charges is influenced by the lifetime of charge carriers and the material's symmetry. Perovskite oxides are materials that have a high symmetry and are typically characterized by a long carrier lifetime [80]. However, the rapid recombination of photogenerated charges remains a persistent issue with perovskite oxides, limiting the range of photocatalytic processes that can be employed. Hence, it is essential to suppress photogenerated charge recombination during photocatalysis to maximize performance. The mechanism of carrier separation involves two processes. The first occurs constantly without an applied potential gradient, in which carriers move toward the open surface under diffusion

force [81]. In this mechanism, the carriers are in the medium, with the diffusion length providing the distance that the carriers can move away without recombining or scattering, among other phenomena. The second mechanism involves carriers separating at the built-in electric field generated by the potential gradient from the formation of heterojunctions. The electric field is instrumental in separating electrons and holes. Heterojunctions occur when two semiconductors differing in energy gap and electrical geometry are hybridized [82]. The junction interface between the two semiconductors results in more heterojunctions. The variability in heterojunctions between the two different semiconductors explains the need to replace the use of a single photocatalyst, as shown in **Figure 4(a)** [83].

One significant advantage of heterojunctions is their ability to expand the spectrum range for light absorption. Specifically, photocatalysts related to semiconductors cannot absorb more than 45% of visible light, leaving out a large portion of the solar spectra [84]. Heterojunctions are formed across such interfaces as semiconductor-semiconductor, semiconductor-metal, and semiconductor-conducting supports. For example, semiconductor materials may be combined with metal nanoparticles with conducting substrates, e.g., graphene with other semiconductor materials possessing suitable band alignments. This allows charge transfer with high efficiency through the created interfaces [85,86]. Exploring the various charge transfer mechanisms in different types of photocatalytic systems is important. When two semiconductor materials are combined, it results in the emergence of heterojunctions that allow for the adjustment of the charge transfer nature and the light absorption characteristics of the compounds formed, as shown in **Figure 4(b)**. Based on charge transfer, there are mainly three types of heterojunction systems: straddling gap (Type-I heterojunctions), staggered gap (Type-II heterojunctions), and broken type (Type-III heterojunctions). The formation of these types depends on the band position of the semiconductors [87]. This involves heterojunction systems comprising two semiconductor photocatalysts, herein referred to as PC-A and PC-B. In a Type-I heterojunction system, the conduction band of PC-A is significantly more negatively charged compared with that of PC-B, as shown in **Figure 4(c)**. Similarly, the valence band of PC-A is more positively charged than that of PC-B. As a result, when incident light containing photons with energy greater than the bandgap is present, the PC-A component is excited and produces electron-hole pairs in the conduction and valence bands of PC-A. At the same time, PC-A primarily allows photoexcited electrons and holes to move to the surface, where they contribute to oxidative and reductive reactions, respectively. However, Type-I heterojunctions do not spatially separate charge carriers, resulting in the accumulation of electron-hole pairs in the same semiconductor and an increased rate of recombination. Furthermore, photoreactions occur in the semiconductor with a lower oxidation and reduction potential, which aligns with the specified conditions. Therefore, the achievement of photocatalysis is not possible when using light radiation [82].

Type-II heterojunctions are shown in **Figure 4(d)**, where the conduction band and valence band of PC-A are positioned above those of PC-B [87,88]. This arrangement allows for the downward movement of electrons and the upward movement of holes, thereby facilitating the separation of charge carriers. In

heterojunction photocatalysts, electrons accumulate at the less-negative position of the conduction band, while holes accumulate at the less-positive position of the valence band. In the case of the conduction band of PC-A, the valence band of PC-B is positioned below the valence band of PC-A. Consequently, the less-negative valence band allows for the transfer of electrons from PC-A to PC-B [89]. Ultimately, the holes will be transferred from the valence band of PC-A to the valence band of PC-B. On the other hand, the structural configuration of Type-III heterojunctions, as shown in **Figure 4(e)**, may seem similar to that of Type-II heterojunctions; however, since band levels are placed at extreme values, the configuration is without bandgap overlap at the interface [90]. Type-III heterojunctions exhibit a greater disparity in the positions of the valence bands and conduction bands of the two semiconductors compared with those of Type-II heterojunctions. Photogenerated electrons from PC-A undergo recombination with the valence band's holes of PC-B; electrons from PC-B go through redox reactions with the valence band's holes of PC-A [91]. Therefore, when considering the best setup for achieving maximum separation of electrons and holes in a traditional heterojunction system, it is apparent that Type-II heterojunctions are the most suitable choice. A p-n heterojunction photocatalyst is a combination of p-type and n-type semiconductors that facilitates the transfer of unbound electrons from the conduction band of the n-type material to the p-type material upon contract between the two, as shown in **Figure 4(f)** [92]. This phenomenon occurs due to the establishment of oppositely charged boundaries brought about by the shifting of Fermi levels when the semiconductors meet.

In a heterostructure system formed by the joining of p-type and n-type materials, an internal electric field arises at the interface as a result of the diffusion of charge carriers between the distinct types of semiconductors, which induces a potential offset across the contact point of the two materials comprising the photocatalyst [93]. Liao et al. [94] studied the synthesis of a visible-light-driven p-n heterojunction composite of $BiFeO_3$ and TiO_2 by simple hydrolysis and precipitation. They discovered that the $BiFeO_3/TiO_2$ composite demonstrated the highest degradation efficiency of tetracycline, which reached 72.2% after 180 min of visible light illumination. $BiFeO_3$ exhibited a degradation efficiency of 64.9%, whereas the same activity of TiO_2 was lower at 38.3%. Thus, it was concluded that this was due to the synergistic effect of the combination of the two compounds in the composite. Paramanik et al. [95] provided a simple two-step way to construct a new type of $PbTiO_3/LaCrO_3$ p-n heterojunctions, as shown in **Figure 4(g,h)**. Detailed structures of the constructed PT/LC p-n heterojunctions were characterized and resolved. It was found that the p-type $LaCrO_3$ perfectly adhered to the n-type $PbTiO_3$, boasting electronic paths beyond the interface. The presence of heterojunctions between the two metal oxides greatly reduced the number of electrons and holes recombining in the $PbTiO_3/LaCrO_3$ interface, thus enhancing the duration of the p-n junction material. In their work, Li et al. [96] presented a way of creating fiber-shaped Ag_2O/Ta_3N_5 p-n heterojunctions as an efficient photocatalyst, as shown below in **Figure 4(i)**. It was designed by carrying out an in-situ anchoring process of porous Ta_3N_5 nanofibers, in which Ag_2O nanoparticles were embedded. That way, the Ag_2O/Ta_3N_5 composite benefited from the internal electric field naturally generated by the p-n junction. Also, it possessed a hierarchical pore and a high specific surface

area, which is very important in improving photocatalytic activity. Thus, the design was optimally suited for absorbing light and helped in separating charge carriers, ultimately increasing the efficiency of photocatalysis. On the other hand, a Z-scheme is an exciting phenomenon of photocatalysis because it gives rise to photogenerated charges with considerable redox potential [97]. In this case, electrons from the conduction band of PC-B move to the valence band of PC-A, which significantly reduces the likelihood of photo corrosion. Spontaneous recombination of photogenerated electrons and holes in each semiconductor is made possible by the built-in electric field, resulting in highly efficient separation. A Z-scheme implies electrons and holes that can be separated by the interface and possess a high redox power. A visual representation of the direct charge transfer and separation in a Z-scheme is represented in **Figure 4(j)**. A direct Z-scheme photocatalyst facilitates the maximum recombination of electrons from the less-negative conduction band of one semiconductor and the holes from the less-positive valence band of the other [98]. As a result, the high-oxidation-capable holes and the high-reduction-capable electrons are not involved in recombination and are made available to continue any photocatalytic reaction that has begun. This enables the increase of the overall redox potential of the Z-scheme counterpart. Therefore, Z-scheme heterojunctions offer a new approach to increasing photocatalytic performance, while ensuring that excessive electrons and holes are produced all over the redox potential of the whole system. Fu et al. [99] formulated a new mechanism, known as the step scheme (S-scheme), which is based on the principles of the Z-scheme and can be used in a variety of different photocatalytic processes [100–102]. As shown in **Figure 4(k)**, the S-scheme creates heterojunctions between two n-type semiconductors comprising an oxidation photocatalyst and a reduction photocatalyst. The electric field that appears on its own is the driving force of the S-scheme, while the interface closes by itself and the n-type semiconductors make a common facet [103,104]. Systems using the S-scheme provide photogenerated charges with powerful redox properties due to the built-in electric field, providing an efficient transfer of charges at the interface.

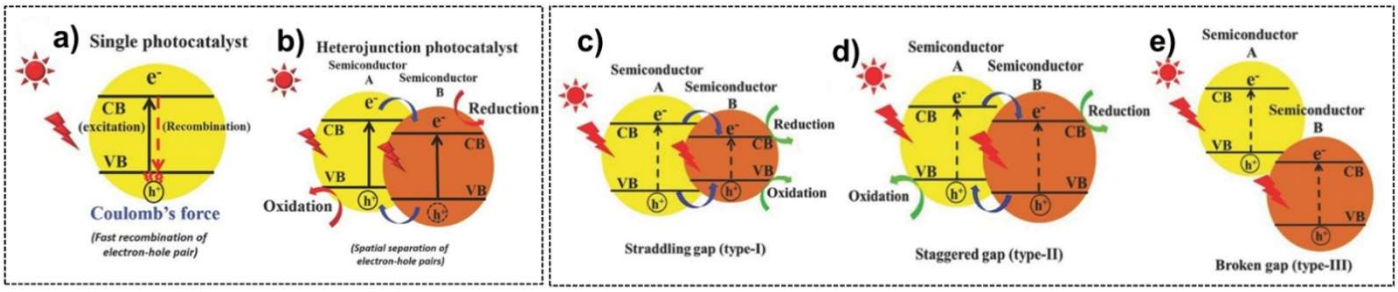

Figure 4. (*Continued*).

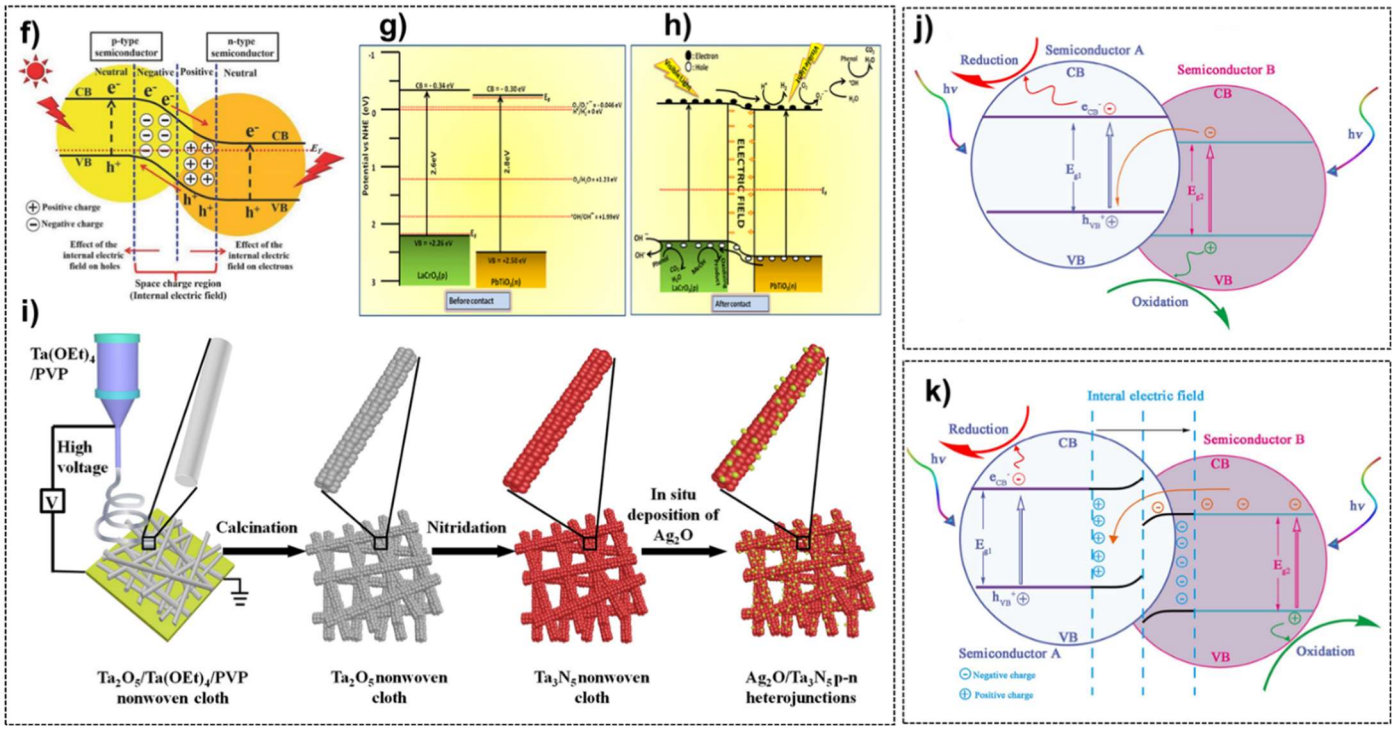

Figure 4. (a) Recombination of electrons and holes on single photocatalyst. **(b)** Separation of electrons and holes on heterojunction photocatalyst. Schematic illustration of three distinct modes of electron-hole pair separation observed in heterojunction photocatalysts: **(c)** Type-I heterojunction configuration. **(d)** Type-II heterojunction configuration. **(e)** Type-III heterojunction configuration. **(f)** Schematic depiction of electron-hole separation within p-n heterojunction photocatalyst [82]. **(g)** Schematic description of formation of p-n heterojunction. **(h)** Proposed charge separation mechanism in $PbTiO_3/LaCrO_3$ under visible light irradiation [95]. **(i)** Fabrication process of fiber-shaped Ag_2O/Ta_3N_5 p-n heterojunctions [96]. **(j)** Separation and transfer of charge carriers across heterojunction intersurface in Z-scheme system. **(k)** Energy band structure and charge transfer in S-scheme photocatalyst featuring internal electric field [105].

2.3.2. Control over crystal structure and morphology

Lattice distortion in perovskites alters their dipole moment and electronic structure. Consequently, distinct crystal fields are formed, which significantly affect the excitation, separation, and transfer of photogenerated charge carriers. In general, crystal structures of high symmetry enhance the lifetime of carriers [106]. Perovskite materials in microstructures and nanostructures possess larger specific surface areas and present many active sites. Moreover, doping and defect engineering effectively induce a distortion of the materials' lattice. Additionally, different synthesis techniques allow the fabrication of the desired perovskite materials with various crystal structures, morphologies, and sizes. As a result, the research on controlled crystal structure and morphology is becoming one of the promising hot spots for perovskite oxides.

3. Understanding photocatalytic processes: Overview and mechanism

In a photocatalytic reaction, when light with sufficient energy ($h\nu \geq E_g$) strikes a semiconductor material, electrons (e^-) are energized from the valence band to the conduction band, creating electron-hole pairs (h^+). This step forms the fundamental

basis for all photocatalytic processes. Specifically, this energy must be sufficient to allow the migration of photogenerated charges to the surface of the photocatalyst, where they participate in redox reactions. These electrons and holes can participate in various photocatalytic reactions, depending on whether their reduction potentials meet the specific requirements of the application. This includes reactions such as organic pollutant degradation, CO_2 reduction, and N_2 fixation. However, these conditions may vary slightly during experiments, as reactions are not universally conducted at pH levels of 0 or 7. Different band structures of various pristine and doped perovskite oxides offer insights into their suitability for diverse photocatalytic applications. In this section, the significance and mechanistic insights are discussed, while an overview of current trends and the necessary criteria for achieving practical applications are also provided.

Bi_2WO_6 is extensively studied for its photocatalytic capabilities in CO_2 reduction, with numerous studies demonstrating its ability to produce CO, CH_4, and CH_3OH under visible light irradiation [107]. Moreover, to boost the photocatalytic efficiency of Bi_2WO_6, various composites have been developed. These composites integrate Bi_2WO_6 with materials such as MoS_2, g-C_3N_4, MXenes, and BiOI, among others. Significantly, 2D-2D heterojunction photocatalysts have garnered significant interest for their expansive surface area and intimate face-to-face interfacial interactions enabled by their sheet-like morphology. These features promote efficient charge transfer, enhancing photocatalytic performance. Cao et al. [108] introduced 2D−2D Bi_2WO_6-MXenes heterojunctions synthesized through a straightforward hydrothermal approach. Ti_3C_2 MXene was derived from its MAX phase and incorporated in varying concentrations as a co-catalyst in Bi_2WO_6-Ti_3C_2 heterojunctions to optimize photocatalytic activity. The heterojunctions exhibited efficient bulk-to-surface and interfacial charge transfer due to the face-to-face interactions between the nanosheets. The high surface area and porous structure of Bi_2WO_6-Ti_3C_2 facilitated effective CO_2 adsorption. Under simulated solar light, the Bi_2WO_6−Ti_3C_2 heterojunctions demonstrated significant photocatalytic activity, yielding CH_4 (1.78 $\mu mol \cdot h^{-1} \cdot g^{-1}$) and CH_3OH (0.44 $\mu mol \cdot h^{-1} \cdot g^{-1}$), which was 4.6 times higher than those of bare Bi_2WO_6 nanosheets. O_2 was produced as an oxidation by-product. In another study, Kong et al. [109] presented a surface-engineered 2D-2D Bi_2WO_6-BiOI photocatalyst for CO_2 reduction. In this study, oxygen-deficient Bi_2WO_6 nanosheets were combined with BiOI nanosheets to create a defect-engineered 2D-2D photocatalyst featuring nanoscale p-n heterojunctions. The presence of oxygen vacancies in Bi_2WO_6 activated the catalyst's surface, enhancing CO_2 molecule adsorption and extending light absorption into the near-infrared region (NIR). Furthermore, the Bi_2WO_6-BiOI p-n heterojunctions, characterized by a rational cascade configuration and internal electric field, promoted directional migration and spatial separation of photogenerated charges, as illustrated in **Figure 5(a)**.

Furthermore, layered Bi_2WO_6 has been investigated for its potential in photocatalytic N_2 fixation. Zhang et al. [110] developed hybrid photocatalysts by combining cyclized polyacrylonitrile (c-PAN) with Bi_2WO_6 (BP), where the unsaturated nitrogen in c-PAN acted as active sites for effective adsorption and activation of N_2 molecules to enhance catalytic efficiency. The optimized catalyst,

BP5, containing 5% c-PAN, exhibited the highest NH_3 production rate of 160 $\mu mol \cdot g^{-1} \cdot h^{-1}$, surpassing pristine Bi_2WO_6. This study exemplifies the effective utilization of surfaces enriched with active sites, which is crucial for N_2 activation and enhancing photocatalytic N_2 fixation performance. X-ray photoelectron spectroscopy (XPS) spectra shown in **Figure 5(b)** confirmed the presence of unsaturated N atoms on the BP5 photocatalyst's surface, which were highly effective in capturing N_2 molecules. Adsorption studies, as shown in **Figure 5(c)**, indicated an extended bond length (1.288 Å) for connected N_2 molecules compared with the N≡N bond (1.078 Å) and diazene's double bond (1.201 Å), affirming successful activation at unsaturated N sites of c-PAN.

Choi et al. [111] investigated the enhancement of photocatalytic CO_2 reduction using a photocatalyst based on inorganic halide perovskite combined with a copper scaffold co-catalyst. This combination significantly improved light absorption, charge separation, and catalytic activity, leading to higher yields of products, such as ethylene (C_2H_4, 46.5 $\mu mol \cdot g^{-1}$) and methane (CH_4, 18.9 $\mu mol \cdot g^{-1}$), compared with those of the perovskite photocatalyst alone. The study employed in-situ ATR-IR analysis to elucidate the photocatalytic CO_2 reduction mechanism. The analysis revealed that the copper scaffold enhanced light harvesting through a multi-scattering process, generating more photo-induced carriers and facilitating efficient electron transfer to active sites. The results underscore the potential of this hybrid system for efficient CO_2 conversion and highlight the critical role of in-situ characterization in understanding underlying mechanisms. Recently, Xu et al. [112] demonstrated a significant enhancement of catalytic performance through the synergistic effect of novel piezoelectric catalysis combined with traditional photocatalysis. They designed novel heterojunction piezo-photocatalysts by integrating Co-N-C and $BiFeO_3$ (BFO), with the Co-N-C@BFO(1:7) catalyst achieving yields of CO_2 reduction to CO and CH_4 reaching 1373.41 $\mu mol \cdot g^{-1}$ and 169.32 $\mu mol \cdot g^{-1}$, respectively. The study elucidated the underlying mechanism through a combination of displacement current, energy band theory, piezoelectric effect, and in-situ DRIFTS analysis. In the piezo-photocatalysis process, the displacement current generated time-varying electrostatic potential, facilitating electron transfer to Co-N-C active sites, thereby promoting CO_2 reduction reactions (CO_2RR). The energy band configuration of BFO aligned with potential requirements, further aiding in electron transfer to Co-N-C active sites. The integration of piezoelectric fields and visible light enhanced charge separation, thus improving catalytic activity. This work offers profound insights and introduces a novel approach for the piezo-photocatalytic reduction of CO_2, contributing to advancements in sustainable energy and environmental remediation.

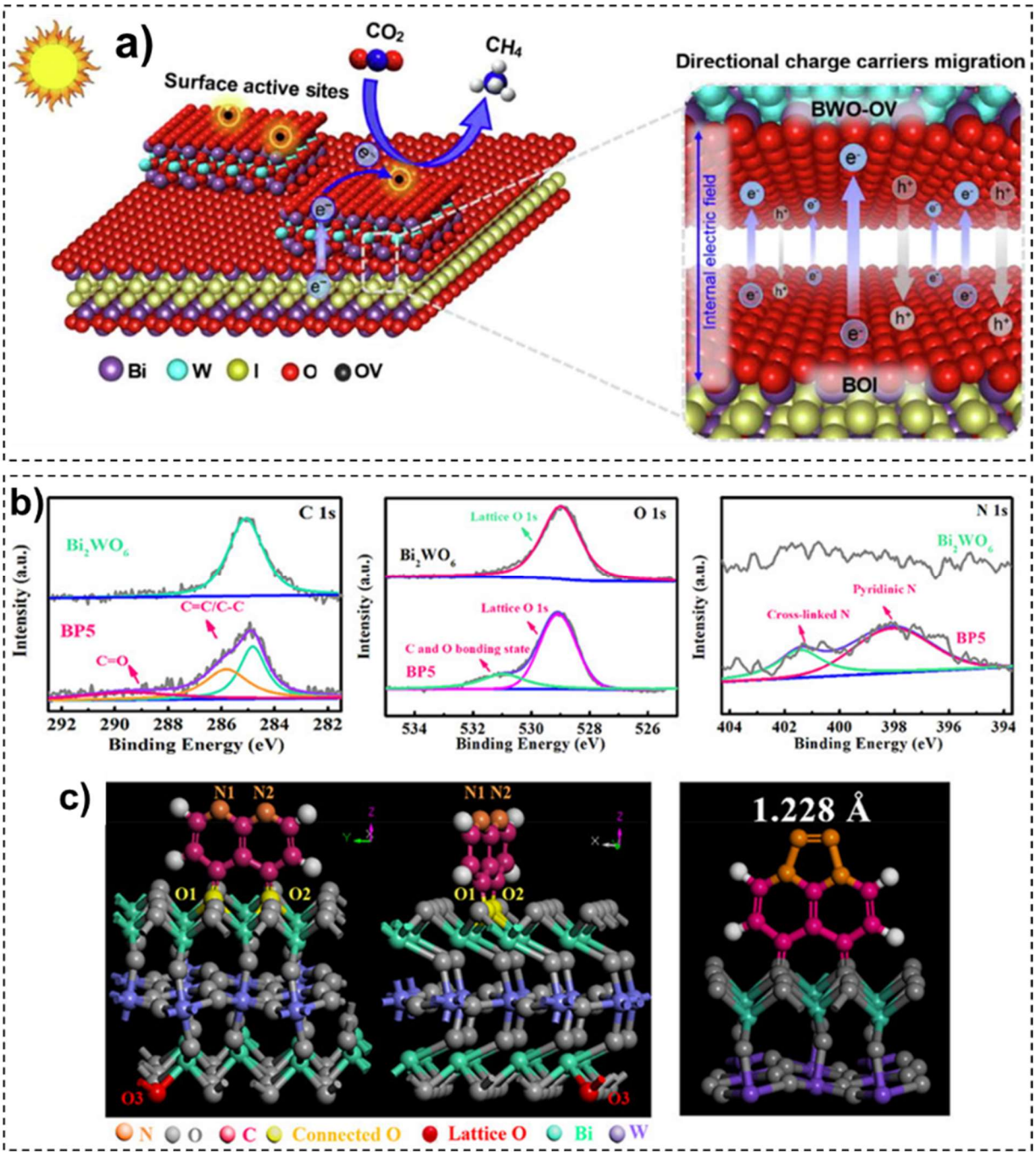

Figure 5. (a) Mechanism of photocatalytic CO_2 reduction in Bi_2WO_6-BiOI p-n heterojunctions, highlighting the impact of oxygen vacancies and directional charge migration [109]. **(b)** XPS spectra of C 1s, O 1s, and N 1s for Bi_2WO_6 and BP5. **(c)** Optimized structure and absorbed N_2 bond length of BP5 [110].

4. Perovskite oxide applications

4.1. CO_2RR

Although fossil fuels have largely facilitated the establishment and enhancement of human societies as one of the primary energy resources, excess utilization has increased CO_2 levels to an alarming point. Moreover, atmospheric CO_2 has surged beyond 400 ppm in recent years and continues to rise by more than 2 ppm every year. Therefore, the reduction of current CO_2 emissions is vital [113]. As

a result, one of the most popular technologies employed for transformation processes involves CO_2 utilization for valuable chemicals or fuels as a carbon source [114]. This has become a sustainable solution to some pressing difficulties, such as energy deficiency and excess, production of clean energy, and strengthening and renewal of the global carbon cycle to maintain environmental stability. However, the high energy of the C-O bond is equal to 750 $kJ \cdot mol^{-1}$, much higher than the energy of the C-H bond of 411 $kJ \cdot mol^{-1}$ or C-C bond of 336 $kJ \cdot mol^{-1}$, resulting in the compound being one of the most stable carbon compounds from the thermodynamics perspective. Thus, the transformation of CO_2 to preferable products is quite difficult [115]. In the natural world, the transformation of CO_2 in the air is associated with photosynthesis, where plants convert CO_2 and water into glucose and oxygen using solar energy. Similarly, when CO_2 is transformed into other chemical forms using semiconductor photocatalysis, the sun's energy is harnessed to drive the reaction. This analogy to natural photosynthesis urges the development and application of semiconductor photocatalysis for CO_2 reduction, with the aim of achieving sustainable energy production and environmental remediation [116].

It is environmentally friendly and more cost-effective to recycle as a medium such as perovskite oxides. Various forms of perovskite oxide catalysts have been used in the light spectra, as shown in **Table 2**, and research in the field of photocatalytic reduction of CO_2 is now one of the most popular research areas. The basic condition required for the CO_2 capacity of a photocatalyst in an aqueous medium is that the maximum valence band energy level of the photocatalyst is lower than the oxidation potential of water, while the minimum conduction band energy level is higher than the reduction potential of CO, to facilitate the generation of reduced products [117]. Considering that photoexcitation and CO_2 activation processes can be enhanced to realize high efficiency and selectivity, metal oxides have gained more attention due to their availability of surficial and bulk properties. Perovskite oxide materials excel owing to their special crystal structure, which results in the variation of the radius of metal atoms and manipulation of two metal ions via defect engineering. Furthermore, perovskite oxides have desirable physicochemical characteristics, such as the bottom of their conduction band favoring CO_2 reduction, as well as high carrier mobility, which make them suitable for the photocatalytic transformation of CO_2 [114]. The photocatalytic reduction of CO_2 using perovskite oxides involves several crucial steps, as described in **Figure 6**. The process begins with the adsorption of CO_2 molecules on the perovskite's surface with a physically driven adsorption process. The photons then excite electrons within the perovskite, leading to the generation of electron-hole carrier pairs. The photoexcited pairs then separate and migrate to the catalyst's surface for redox reactions brought about by the reactants. Finally, the reaction products are desorbed from the surface. Notably, the steps are crucial in enhancing catalysis, as they prevent charge recombination. Furthermore, approaches such as the loading of a co-catalyst and heterojunction design are vital in ensuring that charge recombination is minimized, thus enhancing photocatalysis efficiency [118].

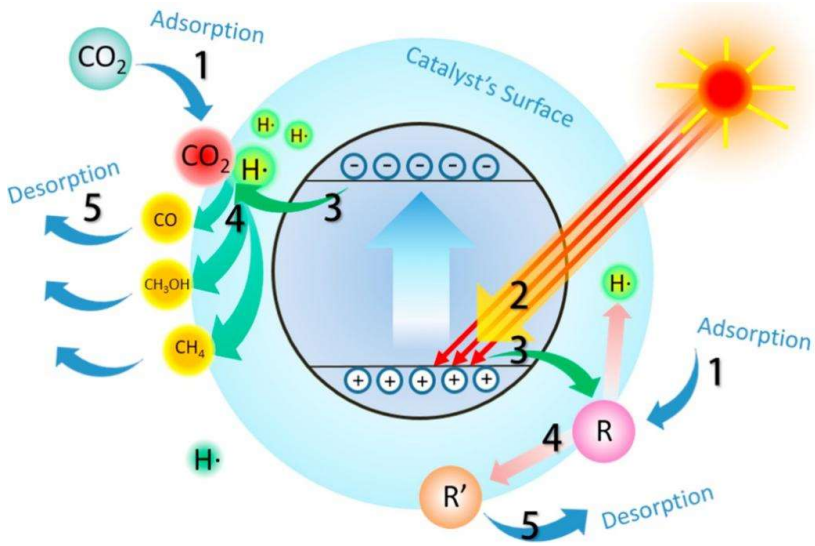

Figure 6. Schematic description of steps involved in photocatalytic CO_2 reduction to CO, CH_3OH, and CH_4 [119].

Table 2. Perovskite oxide catalysts for photocatalytic conversion of CO_2 into various value-added products.

Photocatalyst	Source of light	Chemical reaction condition	Product involved	Ref.
$KTaO_3$	UV-Vis	CO_2+H_2O	CO	[120]
$CaTiO_3$	UV-Vis	CO_2+H_2O	CO	[121]
Pt-$SrTiO_3$	UV-Vis	CO_2+H_2O	CH_4	[122]
$LiTaO_3$	UV-Vis	CO_2+H_2	CO	[123]
Rh-$SrTiO_3$	300W Xenon lamp	CO/CO_2+H_2O	CH_3OH	[124]
Pt-C_3N_4-$KNbO_3$	300W Xenon lamp	CO_2+H_2O	CH_4	[125]
$PbTiO_3$-basalt	UV-Vis	CO_2+H_2O	CH_4	[126]
$BiWO_6$	300W Xenon lamp	CO_2+H_2O	CH_3OH	[107]
$BaZrO_3$	UV-Vis	CO_2+H_2O	CH_4	[127]
C-doped $LaCoO_3$	300W Xenon lamp	CO_2+H_2O	HCOOH	[128]
$NaNbO_3$	UV-Vis	CO_2+H_2O	CO	[129]
$BaCeO_3$	300W Xenon lamp	CO_2+H_2O	CH_4	[130]
$CsPbBr_3$	300W Xenon lamp	CO_2+H_2O	CO, CH_4	[131]
$NaTaO_3$	300W Xenon lamp	CO_2+H_2O	CH_4,CO	[132]
$MnCo_2O_4$	300W Xenon lamp	CO_2+H_2O	H_2, CO	[133]

4.2. N_2 fixation

With almost 78% of the earth's atmosphere by volume, nitrogen is one of the simplest substances, yet still serves as an essential component [134]. Nitrogen is the element that makes life possible and vegetation grows, as it is the basis for a myriad of nitrogen-containing compounds. Ammonia, as one of the priority products for agricultural fertilizers and feedstock and for industrial, chemical, and energy carrier industries, is one of the best examples of nitrogen's significance. Nitrogen fixation

appears to be a rather efficient method, as the nitrogen triple bond is considered to be rather inert for making complex nitrogen-containing compounds. In other words, nitrogen fixation appears to be rather effective due to the necessity to overcome quite a high bond energy, which amounts to 941 $kJ \cdot mol^{-1}$ [135]. Due to the absence of valences in the nitrogen molecule, nitrogen gas remains chemically and biologically inert. Nitrogen fixation is a challenging task because of this fact. In the past and up to the present day, the most common method by far to produce ammonia is the traditional Haber-Bosch process [136]. It requires a series of harsh reaction conditions, including high temperatures of 300–500 ℃ and pressures of 20–50 MPa. Moreover, the process demands substantial power consumption and results in greenhouse gas production. The photocatalytic production of NH_3 has attracted substantial attention since the first report by Schrauzer and Guth [15] in 1977 that Fe-doped TiO_2 showed an activity for the conversion of N_2 to NH_3 under UV light irradiation. This method is remarkable because it is energy-efficient, high-yield, and environmentally sustainable [137,138].

The principle of photocatalyst-based nitrogen fixation is shown in **Figure 7(a)** [139]. When light is irradiated on a semiconductor, light-generated electrons are excited. The electrons undergo separation and move to the conduction band of the catalyst. Then, holes in the valence band, which also infiltrate the catalyst's surface, oxidize water. The final reaction on the catalyst's surface is the electrons in the conduction band reacting with nitrogen, which is channelized through active sites and results in ammonia gas. The action is a multistep, whereby electrons and protons are transferred by water and then oxidized to O_2 by intercontiguous holes. As shown in the figure, nitrogen reduction to ammonia can also be caused by two mechanisms: associative and dissociative [140]. From the DFT study by Azofra et al. [141], the dismutation of N_2 implies five routes for the transfer of h^+/e^- pairs, as shown in **Figure 7(b)**. The latter is most widely recognized in both distal and alternating mechanisms. The distal mechanism is characterized by the sequential attachment of h^+/e^- pairs to one N atom of N_2, which thus results in a terminal nitride intermediate and the release of the first molecule of NH_3. Later on, this domain is converted into another product, which is NH_3. In contrast, the alternating mechanism suggests h^+/e^- pairs being added to two N atoms of N_2. In delving into the mechanism of N_2 fixation, employing a blend of experimental exploration and computational modeling facilitates a deeper understanding of reaction pathways. Computational simulations provide prospective directions for guiding further experiments, complemented by experimental investigations that offer feedback and confirmatory insights for optimizing the theoretical model. Investigations into perovskite oxides have shown their promise as highly efficient photocatalysts. The diverse composition and the flexibility of A and B sites of perovskite oxides, along with the tunability of their bandgaps, enable significant enhancements in both the absorption range and catalytic efficiency. However, while doping is a common method to improve the absorption range, it often leads to a reduction in catalytic efficiency by disrupting crystallinity, compromising stability, and increasing carrier recombination.

An oriented structure was designed by Zhou et al. [142], which used an in-situ bismuth reduction strategy, as shown in **Figure 7(c)**. A uniform distribution of crystallographic orientation throughout a polycrystalline sample was the result of this

technique. The oriented structure allowed for the development of tightly interconnected interfaces and transfer channels that were quick and effective. The quantum size efficiency, which raised the bottom of the conduction band, also magnified substrate-generated electron reduction activities. In addition, metal Bi doped into the composite acted as active sites and resulted in the preferred orientation. As a result, the yield of NH_3 was extremely high at around 86.0 $\mu mol \cdot g^{-1} \cdot h^{-1}$. Therefore, preference orientation and incorporating metals as dopants can further advance the design of highly effective photocatalysts. Additionally, noble metals are the most effective choices when using the co-catalyst loading approach. Xing et al. [143] synthesized an $Ag/KNbO_3$ nanocomposite using combined methods of hydrothermal and photo-deposition, as shown in **Figure 7(d)**. The hydrothermal method led to the enhancement of bulk charge separation of $KNbO_3$ due to its high crystallinity, while the decoration of Ag nanoparticles was modified to trap electrons for improved surface charge carrier separation. Moreover, two different mechanisms were found in the $Ag/KNbO_3$ nanocomposite. This is indicative of the role of Ag in facilitating the simulated sunlight and visible light conditions. In addition to doping and introducing co-catalysts, the generation of heterojunctions has become a focus area. $TiO_2/SrTiO_3/g\text{-}C_3N_4$ ternary heterojunction nanofibers, depicted in **Figure 7(e)**, were synthesized using two-phase electrospinning and the gas-solid reaction method [144]. When the TiO_2, $SrTiO_3$, and $g\text{-}C_3N_4$ responded to sunlight, they generated photogenerated electrons and holes, respectively. First, electrons generated in $g\text{-}C_3N_4$ were transmitted to TiO_2 through $SrTiO_3$. Subsequently, $SrTiO_3$ also pushed electrons into TiO_2. Conversely, holes generated in TiO_2 and $SrTiO_3$ were then transferred to $g\text{-}C_3N_4$ through a similar method. Finally, the gradient-energy-band heterojunctions of the $TiO_2/SrTiO_3/g\text{-}C_3N_4$ nanofibers heightened the cascade-driven charge transfer. As a result, further separation of the photon-generated carriers was imminent. Moreover, an extensive study indicated that fibers with a one-dimensional structure manifested a heightened specific surface area. Therefore, the $TiO_2/SrTiO_3/g\text{-}C_3N_4$ nanofibers exhibited better photocurrent response and a decrease in transient photoluminescence lifetime. The $CeO_2\text{-}BiFeO_3$ p-n heterojunction photocatalyst showed a remarkable N_2 fixation performance, with a N_2 fixation rate of 117.77 $\mu mol \cdot g^{-1} \cdot h^{-1}$, which was ascribed to the formation of oxygen vacancies and built-in electric field within the $CeO_2\text{-}BiFeO_3$ p-n heterojunction photocatalyst, as shown in **Figure 7(f,g)**. Surface modification is also a key approach to realizing expected catalytic performance, attributed mainly to active site introduction and surface feature change [145]. Few studies have explored perovskite-based materials for N_2 fixation. Primarily, some photocatalytic materials, such as $SrTiO_3$, $KNbO_3$, $LaCoO_3$, and layered Bi_2WO_6, have been utilized for N_2 fixation, as discussed previously and summarized in **Table 3**.

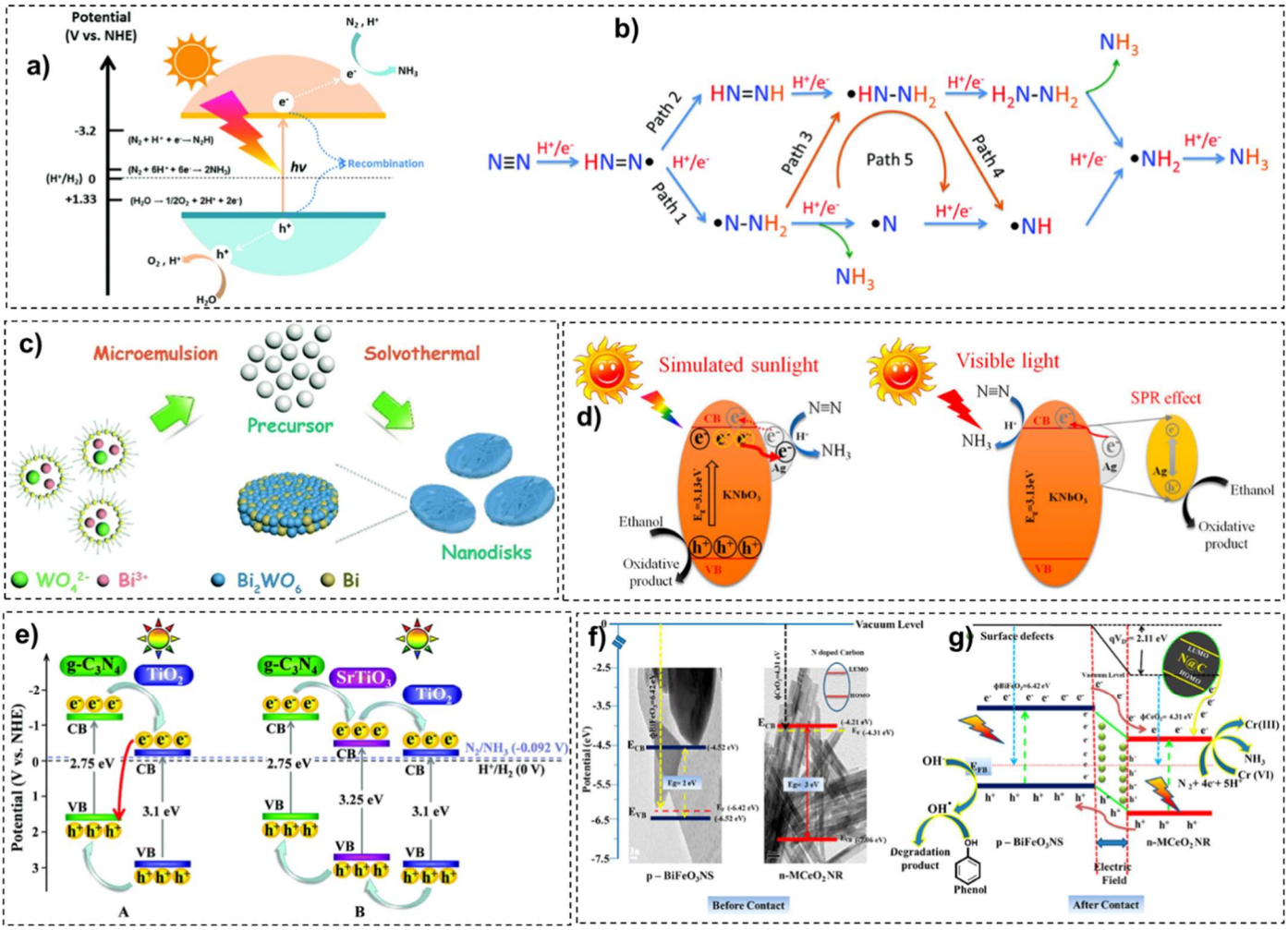

Figure 7. (a) Schematic illustration of use of semiconductor-based photocatalysts for N_2 to NH_3 [139]. **(b)** Proposed pathways for N_2 conversion process [141]. **(c)** Schematic depiction outlining proposed formation mechanism of Or-Bi/Bi_2WO_6 [142]. **(d)** Potential mechanisms observed in Ag/$KNbO_3$ composite under simulated sunlight and visible light irradiation [143]. **(e)** Photocatalytic pathways of (A) TiO_2/g-C_3N_4 and (B) TiO_2/$SrTiO_3$/g-C_3N_4 heterojunctions under simulated solar irradiation [144]. **(f,g)** Charge transfer dynamics across p-n junction in $MCeO_2$-$BiFeO_3$ composite [145].

Table 3. Summary of perovskite oxides used for N_2 fixation.

Photocatalyst	Light source	Sacrificial agent	NH_3 production rate	Ref.
Bi-Bi_2WO_6	Simulated solar light	None	86.0 μmol·g^{-1}·h^{-1}	[145]
c-PAN-Bi_2WO_6	Simulated solar light	None	160.0 μmol·g^{-1}·h^{-1}	[110]
TiO_2/$SrTiO_3$/g-C_3N_4	Simulated solar light	Ethanol	2192.0 μmol·g^{-1}·h^{-1}	[144]
CeO_2-$BiFeO_3$	UV-Vis	None	117.77 μmol·g^{-1}·h^{-1}	[146]
Ag-$KNbO_3$	Simulated solar light	Ethanol	385.0 μmol·g^{-1}·h^{-1}	[143]
$LaCoO_3$.Er^{3+}/ATP	Visible	Ethanol	71.5 μmol·g^{-1}·h^{-1}	[147]

5. Single-atom catalysts (SACs)

A conventional example of enhancing semiconductor photocatalysts is to deposit metal nanoparticles or clusters onto a semiconductor, enabling outstanding catalytic activity and specific product selectivity. Although this method is advantageous in terms of ease of synthesis, capacity of a large amount of metal

loading, and flexible structural design, it has intrinsic obstruction of active site limitation and excessive consumption of metal, especially precious metals, and is not suitable to be used on a large scale in the future. To overcome these obstacles, it is an essential strategy to minimize the co-catalyst to single atoms to provide enough active sites with the highest possible accessibility. Thus, it is possible to achieve prominent enhancements in photocatalytic performance and reduction of material use [148]. In 2011, Qiao et al. [149] developed single-atom Pt/FeO_x catalysts, pioneering the concept of single-atom catalysts (SACs). The primary characteristic of SACs is the uniform distribution of co-catalysts (noble or non-precious metals) as individual atoms across the surface of the semiconductor support. This arrangement ensures maximum atomic efficiency, with isolated single atoms serving as active centers [150]. In the past few years, a significant number of SACs have been prepared and characterized, prompting significant investigation of the nature of their active sites and the mechanisms of catalytic reactions [151]. Conventional nanoparticles, clusters, and bulk materials, for example, have far more unsaturated coordination and electronic structures than SACs. This study discovered that SAC mergers that have taken place in recent years have paved the way for improvements in the absorption and activation of reactants, in addition to the transition of carriers and the level of catalytic activity [152]. Huang et al. [153] reported that a single atom covalent triazine-based frameworks (CTFs) Co/CTF catalyst achieved a remarkable CO_2 absorption capacity of 11.37 $cm^3 \cdot g^{-1}$, surpassing the performance of a Co-NP/CTF catalyst. Additionally, when a CO_2 reduction photocatalysis test was conducted, the desorption rate of CO from a catalytic bed for single atom Co/CTF was determined as 1665.74 $\mu mol \cdot g^{-1} \cdot h^{-1}$, exceedingly significantly the CO yield for CO-NP/CTF, which was 13.29 $\mu mol \cdot g^{-1} \cdot h^{-1}$. To sum up, it should be noted that SACs have several advantages. First, their unsaturated coordination environment and unique electronic structure can change the adsorption and desorption performance of each reaction, specifically, the adsorption performance refers to the ability of SACs to capture reactants, intermediates, and products on their surface while desorption performance relates to how easily these species are released, thus SACs can enhance both catalytic performance and selectivity. Second, SACs allow atomic utilization to reach a maximum; that is, a minimum amount of metal can minimize the number of active sites. Third, SACs can become a universal platform that may be utilized for exploring relationships between activity and structure in multiphase catalysis at the atomic/molecular scale. Last but not least, SACs exhibit a uniform active-site distribution and can maintain non-homogeneous catalysts' solid structure. Such a mixture can be used to develop a sustainable catalytic reaction technology in an ideal direction [154]. Concerning the photocatalytic mechanism, it is interesting to state that SACs show significant influence on the three pivotal steps mentioned above, thanks to their strong interaction with the supporting material. In this broad meaning, SACs are capable of changing the energy band structure of semiconductors used in substrates and redistributing electrons. For example, the intermediate energy band generation makes the photo response spectrum wider and operates as electron traps, and thus charge separation and directed transfer are more efficient [155].

In the recent past, the development of SACs has emerged as an exciting research area, though their application in photocatalysis is still in the early stages.

This emerging multidisciplinary field demands increased attention and effort from the scientific community. This part of the review outlines the instrumental role of SACs in influencing the light absorption of photocatalysts, charge transfer kinetics, and interfacial reactions in order to develop a better understanding of the mechanisms of the activity-structure relationship in SAC-based photocatalytic systems. In addition, the work emphasizes the broad range of applications of multi-phase SACs in several critical energy conversion processes and the improvement of the environment through the reduction of CO_2.

5.1. Role of single atoms in photocatalytic process

5.1.1. Band structure adjustment

As of today, SACs have achieved good results, but their application in photocatalysis is still in its infancy, making it an emerging field of interdisciplinary concern. However, a key factor in photocatalysis is the formation of electron-hole pairs by absorbing light, and the photocatalytic material's ability to absorb light is a vital factor in assessing its performance in the process. Some semiconductor materials boast large bandgaps but their photoactivity is limited to UV light. Unfortunately, only 5% of sunlight falling on the surface of the earth is UV light, and hence this requires the development of materials with narrower bandgap that are capable of using visible light and even near-infrared. Typically, the bonding of single atoms can affect a substrate's band structure, thus increasing its redox ability and light-absorbing capabilities. For example, when electronic atoms of metals, such as Pt, Pd, Rh, or Ru, adhere to the surface of anatase TiO_2, the addition of the metal atoms pushes the conduction band (CB) edge of TiO_2 upward, thereby increasing the reduction potential [156]. Interestingly, the introduction of confined noble metal (NM) single atoms into g-C_3N_4 led to a downward shift of the conduction band, causing it to intersect the Fermi level, as shown in **Figure 8(a)** [157]. Consequently, the bandgap of the NM_1/g-C_3N_4 system narrowed, thereby enhancing its responsiveness to visible light. This phenomenon was also observed in other studies investigating the impact of NM single atoms on the bandgap of single-layer g-C_3N_4 (S-g-C_3N_4). Specifically, the bandgap of g-C_3N_4 decreased from 1.18 eV to 0.72 eV upon Pt single-atom loading, and the attachment of Pt single atoms onto S-g-C_3N_4 further reduced the bandgap from 1.04 eV to 0.54 eV [158]. Additionally, the loading capacity of single atoms was found to potentially correlate with the bandgap and CB potential of C_3N_4. Xin et al. [159] investigated the impact of loading Ag single atoms on the photocatalytic performance of Ag/C_3N_4. In **Figure 8(b)**, the bandgap of Ag/C_3N_4 samples exhibited a reduction compared with that of the original C_3N_4, further diminishing with higher Ag loading. Additionally, the CB potential of Ag/C_3N_4 displayed a distribution resembling a volcano with varying Ag loading, all showing a more negative CB potential than that of the original C_3N_4. At 0.53% Ag loading, Ag0.53/C_3N_4 SACs exhibited the most negative CB potential, indicating enhanced generation of photogenerated electrons with strong reducing ability, thereby promoting the production of superoxide radicals. Superoxide radicals are well-known active species in degrading macromolecular organic compounds. As a result, the degradation rates of rhodamine B (RhB) and tetracycline (TC) by a

catalyst increased by approximately 165.3 times and 24.9 times, respectively. Similarly, Xiong et al. [160] observed that Ni-SA-*x*/ZrO_2 featured a narrower bandgap compared with that of pristine p-ZrO_2, with the trend intensifying with increased Ni SAC loading.

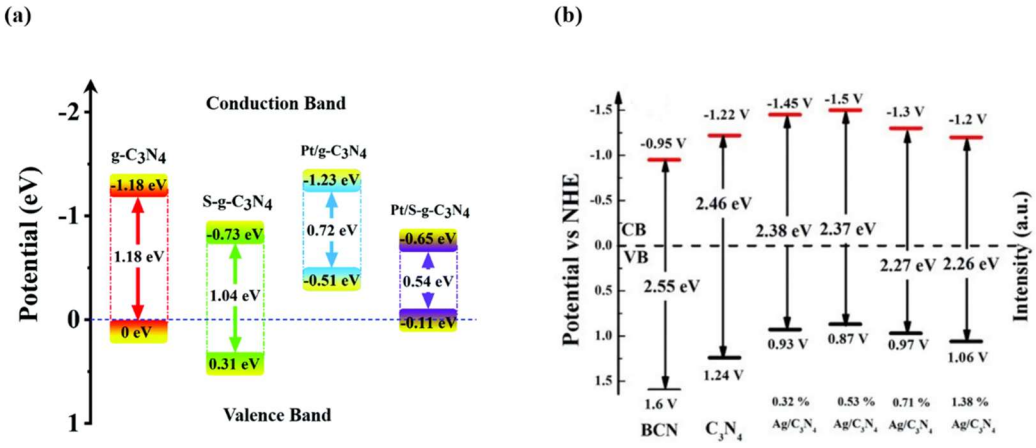

Figure 8. (a) Band structure of different single-atom photocatalysts [158]. **(b)** Bulk Carbon Nitride (BCN), C_3N_4, Ag0.32%/C_3N_4, Ag0.53%/C_3N_4, Ag 0.71%/C_3N_4, and Ag1.38%/C_3N_4 [159].

5.1.2. Promotion of carrier separation and conduction

SACs serve as mediators for electron transfer, establishing pathways for directed charge transfer to enhance the separation and mobility of photogenerated carriers [161]. For instance, Gao et al. [162] developed a core-shell TiO_2@g-C_3N_4(TCN) photocatalyst featuring Pd channels. Introducing metal single atoms onto photocatalysts alters their inherent local electron density, leading to an accumulation of electrons around the metal single atoms [163].

5.2. Application of single-atom photocatalysts in energy conversion and environmental protection

SACs have garnered significant interest because of their optimal atom utilization and distinctive local electronic environment. SACs have shown remarkable effects on three crucial steps of photocatalytic reactions, leading to significant advancements in energy conversion and environmental protection in recent years. In this section, the research progress of single-atom photocatalysts in various areas, such as CO_2 reduction, water splitting, N_2 fixation, air pollutant removal, and water pollutant degradation, are reviewed. The intensified global greenhouse effect and frequent extreme weather in recent years can be attributed to large-scale CO_2 emissions. Utilizing photocatalysis technology can transform atmospheric CO_2 into valuable chemicals and fuels without consuming additional energy, thus simultaneously alleviating global environmental problems and the energy crisis. TiO_2 possesses several advantages, including high stability, low cost, and environmental friendliness. Additionally, it features a large number of atomic step sites with superior electron transfer activity and molecular capture ability. Feng et al. [164] demonstrated the anchoring of single tungsten atomic sites on the TiO_2 atomic step, forming W^{5+}-O-Ti^{3+} active sites for CO_2 photocatalytic reduction. Single

tungsten atomic oxide (STAO) was deposited by adding or replacing Ti atoms on spherical anatase TiO_2 nanoparticles with abundant steps. The loading of Ti^{3+} increased from 0.76% to 9.5% as the loading capacity of STAO increased from 0 wt% to 3 wt%, indicating that STAO anchored in a local coordination environment induced a chemical change from Ti^{4+}-O to Ti^{3+}-O.

5.2.1. CO_2 reduction reaction

Photocatalytic CO_2 reduction using semiconductors has demonstrated potential for artificial photosynthesis. In 1978, single-crystal gallium phosphide was found to convert CO_2 into formic acid, formaldehyde, and methane when exposed to ultraviolet light [165]. Artificial photosynthesis is promising because it can simultaneously reduce global CO_2 accumulation and produce sustainable fuels to meet increasing energy demands. The CO_2 reduction process involves multiple proton-coupled electron transfers and generates various products, such as carbon monoxide, methanol, methane, and higher hydrocarbons. The distribution of these end products is influenced by the kinetic and thermodynamic parameters of the CO_2 reduction pathway. However, despite numerous semiconductor photocatalysts being reported for CO_2 photoreduction, most exhibit low conversion efficiency and lack controlled selectivity. Because metal single atoms have a strong affinity for CO_2 molecules, they can be anchored on a substrate to serve as sites for photocatalytic CO_2 reduction. For instance, Gao et al. [166] demonstrated the feasibility of using Pt and Pd single atoms on g-C_3N_4 for photocatalytic CO_2 reduction through DFT calculations. Reaction potential calculations indicated that HCOOH was the preferred product for CO_2 reduction for Pd/g-C_3N_4 catalysts, with a potential barrier of 0.66 eV. In contrast, CO_2 reduction for Pt/g-C_3N_4 catalysts efficiently produced CH_4, with a potential barrier of 1.16 eV.

5.2.2. Nitrogen fixation

Zhao et al. [167] studied the catalytic activity of transition metal (V, Cr, Mn, Fe, Co, Ni, Cu, Ag, Au, Pd, Pt, and Nb) single atoms on anatase TiO_2(001) systems for nitrogen reduction using DFT calculations. The results demonstrated that Fe single atoms on anatase TiO_2(001) exhibited effective N_2 fixation and NH_3 dissociation activity under mild conditions. Additionally, it was suggested that the alternate pathway of N_2* + H* → NNH* as the determining step was more likely the route for NH_3 generation rather than distal and enzymatic pathways. Wu et al. [168] found that modifying macro/mesoporous TiO_2-SiO_2 (Fe-T-S) with Fe single atoms significantly enhanced photocatalytic nitrogen fixation, achieving a high ammonia yield rate without the need for a sacrificial agent or co-catalyst. Under illumination, photogenerated holes facilitated the transformation of Fe into Fe(IV) species, which enhanced water oxidation and facilitated the hydrogenation of N_2 on nearby oxygen vacancies. Wang et al. [169] anchored Pt single atoms onto covalent triazine framework nanosheets. Ammonia was synthesized from a nitrogen-saturated aqueous solution at a rate of 171.40 $\mu mol \cdot g^{-1} \cdot h^{-1}$ in the absence of a sacrificial agent, with an apparent quantum efficiency of 1.4% at 420 nm. Under light conditions, the conduction band potential of Pt-SACs/CTF facilitated the ammonia synthesis reaction with an N_2/NH_3 potential of −0.28 V vs. NHE, as shown in **Figure 9(a,b)**. Photogenerated electrons from the conduction band of stable ultrathin CTF-PDDA-

TPDH nanosheets could transfer to Pt SACs. This process allowed N_2 molecules adsorbed on Pt SACs to convert to NH_3, which subsequently dissolved in water to form NH^{4+}. The photocatalytic synthesis of NH_3 shows unsatisfactory efficiency, attributed to the weak bonding between N_2 and the photocatalyst, along with the significantly low production efficiency of hydrogen species (H^+) in aqueous solutions. Yin et al. [170] developed Ru-SA/H_xMoO_{3-y} hybrids containing abundant Mo^{n+} adjacent oxygen vacancies through an H-spillover process. These hybrids facilitated the production of NH_3 from N_2 and H_2 atmospheres under ambient conditions. In **Figure 9(c)**, the bandgap of Ru-SA/H_xMoO_{3-y} was observed to decrease significantly, from 3.05 to 2.50 eV, compared with that of MoO_3. This reduction was further enhanced to 1.07 eV, down from 2.05 eV, due to the presence of defect bands created by oxygen vacancies and localized electrons on the *d* orbitals of low-valent Mo species. The synergistic effects of dual active centers, which were Ru single atoms and Mo^{n+}, were instrumental in NH_3 synthesis: Ru single atoms facilitated H_2 dissociation, while oxygen-vacancy-induced Mo^{n+} species acted as sites for electron capture and N_2 adsorption/dissociation. Additionally, oxygen vacancies facilitated the transfer of H^+ from Ru single-atom sites to H_xMoO_{3-y}, effectively preventing Ru single atoms from being poisoned by H_2. Under light irradiation, this system achieved an NH_3 formation rate of 4.0 mmol·h^{-1}·g^{-1} with a quantum efficiency of 6.0% at 650 nm.

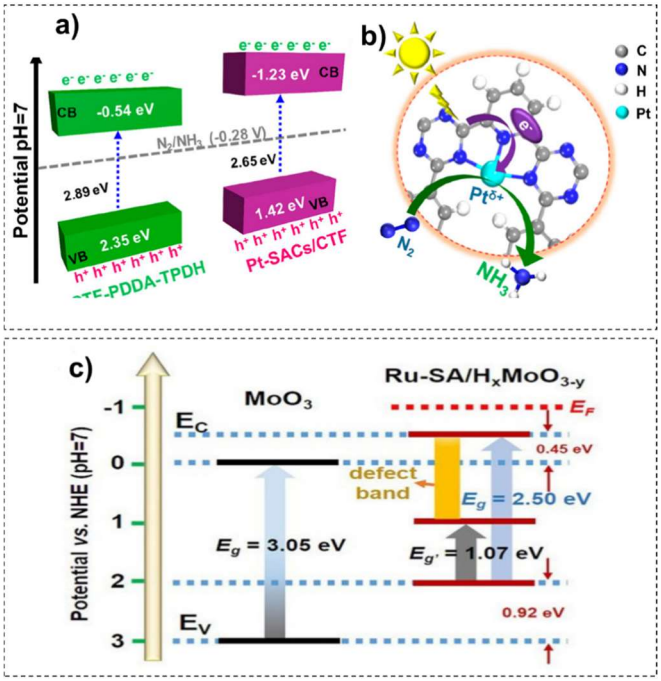

Figure 9. Pt-SACs/CTF: **(a)** band structure and **(b)** N_2 fixation mechanism [171]. **(c)** Band structure of Ru-SA/H_xMoO_{3-y} [170].

6. Summary and outlook

Photocatalysis, leveraging solar energy to address energy and environmental challenges, holds immense promise. Perovskite oxides, emerging as potent photocatalysts, have garnered significant research attention. This review outlines

their structure and synthesis methods, including sol-gel, coprecipitation, hydrothermal, solid-state, and combustion synthesis. It reviews their applications in photocatalysis, spanning hydrogen production, CO_2 reduction, and N_2 immobilization. Researchers have developed various modification techniques to enhance light absorption and photocatalytic performance, such as doping, surface decoration, interfacial and defect engineering, and band structure alignment. However, there is a pressing need for high-efficiency catalysts to improve selectivity and performance in CO_2 reduction and nitrogen immobilization. Theoretical prediction and high-throughput material genome studies hold promise for selecting, designing, and developing new photocatalysts. Practical photocatalysts should exhibit excellent activity, stability, durability, and cost-effectiveness, necessitating efficient substitutes for noble metals and rare-earth elements. Despite TiO_2 dominating the commercial market, large-scale development of perovskite oxides presents new opportunities. Optimizing synthetic strategies for the mass production of high-quality perovskite photocatalysts is crucial for industrial scalability. Given the global urgency for environmental and energy solutions, perovskite oxide photocatalysts offer a promising pathway toward cleaner and greener energy and environment by analyzing their unique structural features and synthesis techniques. We highlighted their superior catalytic performance and the distinct advantages of single-atom catalysts in enhancing energy conversion processes. This review underscores their pivotal role in sustainable energy and environmental remediation, which advocates for further research to optimize synthesis methods and better understand the underlying mechanisms. This will pave the way for more efficient photocatalytic systems crucial for addressing global energy and environmental challenges.

Conflict of interest: The authors declare no conflict of interest.

References

1. Maeda K. Photocatalytic water splitting using semiconductor particles: History and recent developments. Journal of Photochemistry and Photobiology C: Photochemistry Reviews. 2011; 12(4): 237-268. doi: 10.1016/j.jphotochemrev.2011.07.001
2. Hassan JZ, Zaheer A, Raza A, et al. Au-based heterostructure composites for photo and electro catalytic energy conversions. Sustainable Materials and Technologies. 2023; 36: e00609. doi: 10.1016/j.susmat.2023.e00609
3. Raza A, Rafi AA, Hassan JZ, et al. Rational design of 2D heterostructured photo- & electro-catalysts for hydrogen evolution reaction: A review. Applied Surface Science Advances. 2023; 15: 100402. doi: 10.1016/j.apsadv.2023.100402
4. Shehzad N, Tahir M, Johari K, et al. A critical review on TiO_2 based photocatalytic CO_2 reduction system: Strategies to improve efficiency. Journal of CO_2 Utilization. 2018; 26: 98-122. doi: 10.1016/j.jcou.2018.04.026
5. Santos JI, Cesarin AE, Sales CaR, Triano, et al. Increase of Atmosphere CO_2 Concentration and Its Effects on Culture/Weed Interaction. International Journal of Agricultural and Biosystems Engineering. 2017; 11(6): 419-426.
6. Hassan JZ, Raza A, Qumar U, et al. Recent advances in engineering strategies of Bi-based photocatalysts for environmental remediation. Sustainable Materials and Technologies. 2022; 33: e00478. doi: 10.1016/j.susmat.2022.e00478
7. Danesh Miah Md, Farhad Hossain Masum Md, Koike M. Global observation of EKC hypothesis for CO_2, SO and NO emission: A policy understanding for climate change mitigation in Bangladesh. Energy Policy. 2010; 38(8): 4643-4651. doi: 10.1016/j.enpol.2010.04.022
8. Shi Q, Zhang Y, Li Z, et al. Morphology effects in $MnCeO_x$ solid solution-catalyzed NO reduction with CO: Active sites, water tolerance, and reaction pathway. Nano Research. 2023; 16(5): 6951-6959. doi: 10.1007/s12274-023-5407-6

9. Gu X, Guo S, Zhang Y, et al. Boosting oxygen evolution performance over synergistic Tiara nickel clusters and thin layered double hydroxides. Nano Research Energy. 2024; 3: e9120134. doi: 10.26599/NRE.2024.9120134
10. Li Z, Xu M, Wang J, et al. Boosting Up Electrosynthesis of Urea with Nitrate and Carbon Dioxide via Synergistic Effect of Metallic Iron Cluster and Single-Atom. Small. Published online May 15, 2024. doi: 10.1002/smll.202400036
11. Fowler D, Coyle M, Skiba U, et al. The global nitrogen cycle in the twenty-first century. Philosophical Transactions of the Royal Society B: Biological Sciences. 2013; 368(1621): 20130164. doi: 10.1098/rstb.2013.0164
12. Lan R, Irvine JTS, Tao S. Ammonia and related chemicals as potential indirect hydrogen storage materials. International Journal of Hydrogen Energy. 2012; 37(2): 1482-1494. doi: 10.1016/j.ijhydene.2011.10.004
13. Klerke A, Christensen CH, Nørskov JK, et al. Ammonia for hydrogen storage: challenges and opportunities. Journal of Materials Chemistry. 2008; 18(20): 2304. doi: 10.1039/b720020j
14. Zhang J, Xu L, Yang X, et al. Amorphous $MnRuO_x$ Containing Microcrystalline for Enhanced Acidic Oxygen-Evolution Activity and Stability. Angewandte Chemie International Edition. 2024; 63(33). doi: 10.1002/anie.
15. Schrauzer GN, Guth TD. Photolysis of Water and Photoreduction of Nitrogen on Titanium Dioxide. Journal of the American Chemical Society. 1977; 99(22): 7189-7193. doi: 10.1021/ja00464a015
16. Mao C, Wang J, Zou Y, et al. Anion (O, N, C, and S) vacancies promoted photocatalytic nitrogen fixation. Green Chemistry. 2019; 21(11): 2852-2867. doi: 10.1039/c9gc01010f
17. Koe WS, Lee JW, Chong WC, et al. An overview of photocatalytic degradation: photocatalysts, mechanisms, and development of photocatalytic membrane. Environmental Science and Pollution Research. 2019; 27(3): 2522-2565. doi: 10.1007/s11356-019-07193-5
18. Huang S, Ouyang T, Zheng B, et al. Enhanced Photoelectrocatalytic Activities for CH_3OH-to-HCHO Conversion on Fe_2O_3/MoO_3: Fe-O-Mo Covalency Dominates the Intrinsic Activity. Angewandte Chemie International Edition. 2021; 60(17): 9546-9552. doi: 10.1002/anie.202101058
19. Chen F, Zhang Y, Huang H. Layered photocatalytic nanomaterials for environmental applications. Chinese Chemical Letters. 2023; 34(3): 107523. doi: 10.1016/j.cclet.2022.05.037
20. Yang W, Wang H, Liu R, et al. Tailoring Crystal Facets of Metal–Organic Layers to Enhance Photocatalytic Activity for CO_2 Reduction. Angewandte Chemie International Edition. 2020; 60(1): 409-414. doi: 10.1002/anie.202011068
21. Xiong Q, Shi Q, Gu X, et al. Visible-light S-scheme heterojunction of copper bismuthate quantum dots decorated Titania-spindles for exceptional tetracycline degradation. Journal of Colloid and Interface Science. 2024; 654: 1365-1377. doi: 10.1016/j.jcis.2023.10.141
22. Qin Z, Hu S, Han W, et al. Tailoring optical and photocatalytic properties by single-Ag-atom exchange in $Au_{13}Ag_{12}(PPh3)_{10}Cl_8$ nanoclusters. Nano Research. 2021; 15(4): 2971-2976. doi: 10.1007/s12274-021-3928-4
23. Wang J, Kim E, Kumar DP, et al. Highly Durable and Fully Dispersed Cobalt Diatomic Site Catalysts for CO_2 Photoreduction to CH4. Angewandte Chemie. 2021; 134(6). doi: 10.1002/ange.202113044
24. Zhang Y, Li Z, Zhang J, et al. Nanostructured Ni-MoC_x: An efficient non-noble metal catalyst for the chemoselective hydrogenation of nitroaromatics. Nano Research. 2023; 16(7): 8919-8928. doi: 10.1007/s12274-023-5598-x
25. Jerome MP, Alahmad FA, Salem MT, et al. Layered double hydroxide (LDH) nanomaterials with engineering aspects for photocatalytic CO_2 conversion to energy efficient fuels: Fundamentals, recent advances, and challenges. Journal of Environmental Chemical Engineering. 2022; 10(5): 108151. doi: 10.1016/j.jece.2022.108151
26. Chen Y, Li Y, Chen W, et al. Continuous dimethyl carbonate synthesis from CO_2 and methanol over $Bi_xCe_{1-x}O_\delta$ monoliths: Effect of bismuth doping on population of oxygen vacancies, activity, and reaction pathway. Nano Research. 2021; 15(2): 1366-1374. doi: 10.1007/s12274-021-3669-4
27. Dong S, Cui L, Zhang W, et al. Double-shelled $ZnSnO_3$ hollow cubes for efficient photocatalytic degradation of antibiotic wastewater. Chemical Engineering Journal. 2020; 384: 123279. doi: 10.1016/j.cej.2019.123279
28. Di J, Xiong J, Li H, et al. Ultrathin 2D Photocatalysts: Electronic-Structure Tailoring, Hybridization, and Applications. Advanced Materials. 2017; 30(1). doi: 10.1002/adma.201704548
29. Zhang J, Zhang M, Sun R, et al. A Facile Band Alignment of Polymeric Carbon Nitride Semiconductors to Construct Isotype Heterojunctions. Angewandte Chemie International Edition. 2012; 51(40): 10145-10149. doi: 10.1002/anie.201205333
30. Zhu J, Li H, Zhong L, et al. Perovskite Oxides: Preparation, Characterizations, and Applications in Heterogeneous Catalysis. ACS Catalysis. 2014; 4(9): 2917-2940. doi: 10.1021/cs500606g

31. Zhang G, Liu G, Wang L, et al. Inorganic perovskite photocatalysts for solar energy utilization. Chemical Society Reviews. 2016; 45(21): 5951-5984. doi: 10.1039/c5cs00769k
32. Zeng S, Kar P, Thakur UK, et al. A review on photocatalytic CO_2 reduction using perovskite oxide nanomaterials. Nanotechnology. 2018; 29(5): 052001. doi: 10.1088/1361-6528/aa9fb1
33. Kong J, Yang T, Rui Z, et al. Perovskite-based photocatalysts for organic contaminants removal: Current status and future perspectives. Catalysis Today. 2019; 327: 47-63. doi: 10.1016/j.cattod.2018.06.045
34. Hu Y, Mao L, Guan X, et al. Layered perovskite oxides and their derivative nanosheets adopting different modification strategies towards better photocatalytic performance of water splitting. Renewable and Sustainable Energy Reviews. 2020; 119: 109527. doi: 10.1016/j.rser.2019.109527
35. Attfield JP, Lightfoot P, Morris RE. Perovskites. Dalton Transactions. 2015; 44(23): 10541-10542. doi: 10.1039/c5dt90083b
36. Chen D, Chen C, Baiyee ZM, et al. Nonstoichiometric Oxides as Low-Cost and Highly-Efficient Oxygen Reduction/Evolution Catalysts for Low-Temperature Electrochemical Devices. Chemical Reviews. 2015; 115(18): 9869-9921. doi: 10.1021/acs.chemrev.5b00073
37. Zhu Y, Zhou W, Shao Z. Perovskite/Carbon Composites: Applications in Oxygen Electrocatalysis. Small. 2017; 13(12). doi: 10.1002/smll.201603793
38. Wang Q, Yuan Y, Li C, et al. Research Progress on Photocatalytic CO_2 Reduction Based on Perovskite Oxides. Small. 2023; 19(38). doi: 10.1002/smll.202301892
39. Sun YR, Zhang X, Wang LG, et al. Lattice contraction tailoring in perovskite oxides towards improvement of oxygen electrode catalytic activity. Chemical Engineering Journal. 2021; 421: 129698. doi: 10.1016/j.cej.2021.129698
40. Li S, Bai L, Ji N, et al. Ferroelectric polarization and thin-layered structure synergistically promoting CO_2 photoreduction of Bi_2MoO_6. Journal of Materials Chemistry A. 2020; 8(18): 9268-9277. doi: 10.1039/d0ta02102d
41. Yu H, Huang H, Reshak AH, et al. Coupling ferroelectric polarization and anisotropic charge migration for enhanced CO_2 photoreduction. Applied Catalysis B: Environmental. 2021; 284: 119709. doi: 10.1016/j.apcatb.2020.119709
42. Kumar A, Kumar A, Krishnan V. Perovskite Oxide Based Materials for Energy and Environment-Oriented Photocatalysis. ACS Catalysis. 2020; 10(17): 10253-10315. doi: 10.1021/acscatal.0c02947
43. Li Y, Chen G, Zhou C, et al. Photocatalytic Water Splitting Over a Protonated Layered Perovskite Tantalate $H_{1.81}Sr_{0.81}Bi_{0.19}Ta_2O_7$. Catalysis Letters. 2008; 123(1-2): 80-83. doi: 10.1007/s10562-008-9397-5
44. Sorkh-Kaman-Zadeh A, Dashtbozorg A. Facile chemical synthesis of nanosize structure of Sr_2TiO_4 for degradation of toxic dyes from aqueous solution. Journal of Molecular Liquids. 2016; 223: 921-926. doi: 10.1016/j.molliq.2016.09.016
45. Tao Y, Wu L, Zhao X, et al. Strong Hollow Spherical La_2NiO_4 Photocatalytic Microreactor for Round-the-Clock Environmental Remediation. ACS Applied Materials & Interfaces. 2019; 11(29): 25967-25975. doi: 10.1021/acsami.9b07216
46. Machida M, Yabunaka J ichi, Kijima T. Synthesis and Photocatalytic Property of Layered Perovskite Tantalates, $RbLnTa_2O_7$ (Ln = La, Pr, Nd, and Sm). Chemistry of Materials. 2000; 12(3): 812-817. doi: 10.1021/cm990577j
47. Oshima T, Lu D, Maeda K. Preparation of Pt-Intercalated $KCa_2Nb_3O_{10}$ Nanosheets and Their Photocatalytic Activity for Overall Water Splitting. ChemNanoMat. 2016; 2(7): 748-755. doi: 10.1002/cnma.201600072
48. Ida S, Okamoto Y, Matsuka M, et al. Preparation of Tantalum-Based Oxynitride Nanosheets by Exfoliation of a Layered Oxynitride, $CsCa_2Ta_3O_{10-x}N_y$, and Their Photocatalytic Activity. Journal of the American Chemical Society. 2012; 134(38): 15773-15782. doi: 10.1021/ja3043678
49. Shi R, Waterhouse GIN, Zhang T. Recent Progress in Photocatalytic CO_2 Reduction Over Perovskite Oxides. Solar RRL. 2017; 1(11). doi: 10.1002/solr.201700126
50. Chen Y, Gu X, Guo S, et al. Enhancing the Performance of 2D Ni-Fe Layered Double Hydroxides by Cabbage-Inspired Carbon Conjunction for Oxygen Evolution Reactions. ChemSusChem. Published online May 23, 2024. doi: 10.1002/cssc.202400309
51. Zhang J, Raza A, Zhao Y, et al. Intrinsically robust cubic $MnCoO_x$ solid solution: Achieving high activity for sustainable acidic water oxidation. Journal of Materials Chemistry A. 2023; 11(46): 25345-25355. doi: 10.1039/d3ta05233h
52. Gong X, Shi Q, Khalid MS, et al. Configuration Effect of Plasmonic Vanadium–Titanium Solid Solutions for Photo-oxidation of Benzyl Alcohol. ACS Applied Nano Materials. 2024; 7(2): 2062-2071. doi: 10.1021/acsanm.3c05332
53. Yamaguchi Y, Hamamoto K, Hamao N, et al. Near room temperature synthesis of perovskite oxides. Ceramics International. 2019; 45(18): 24936-24940. doi: 10.1016/j.ceramint.2019.08.205

54. Parida KM, Reddy KH, Martha S, et al. Fabrication of nanocrystalline $LaFeO_3$: An efficient sol–gel auto-combustion assisted visible light responsive photocatalyst for water decomposition. International Journal of Hydrogen Energy. 2010; 35(22): 12161-12168. doi: 10.1016/j.ijhydene.2010.08.029
55. Salavati-Niasari M, Soofivand F, Sobhani-Nasab A, et al. Synthesis, characterization, and morphological control of $ZnTiO_3$ nanoparticles through sol-gel processes and its photocatalyst application. Advanced Powder Technology. 2016; 27(5): 2066-2075. doi: 10.1016/j.apt.2016.07.018
56. Ebina Y, Sakai N, Sasaki T. Photocatalyst of Lamellar Aggregates of RuO_x-Loaded Perovskite Nanosheets for Overall Water Splitting. The Journal of Physical Chemistry B. 2005; 109(36): 17212-17216. doi: 10.1021/jp051823j
57. Kwak BS, Do JY, Park NK, et al. Surface modification of layered perovskite Sr_2TiO_4 for improved CO_2 photoreduction with H2O to CH4. Scientific Reports. 2017; 7(1). doi: 10.1038/s41598-017-16605-w
58. Sanwal P, Raza A, Miao YX, et al. Advances in coinage metal nanoclusters: From synthesis strategies to electrocatalytic performance. Polyoxometalates. 2024; 3(3): 9140057. doi: 10.26599/pom.2024.9140057
59. Kalaiselvi CR, Senthil TS, Shankar MV, et al. Solvothermal fusion of Ag- and N-doped $LiTaO_3$ perovskite nanospheres for improved photocatalytic hydrogen production. Applied Organometallic Chemistry. 2021; 35(6). doi: 10.1002/aoc.6207
60. Dawi EA, Padervand M, Ghasemi S, et al. Multi-functional fluorinated $NiTiO_3$ perovskites for CO_2 photocatalytic reduction, electrocatalytic water splitting, and biomedical waste management. Journal of Water Process Engineering. 2023; 54: 103979. doi: 10.1016/j.jwpe.2023.103979
61. Azad AM, Subramaniam S. Synthesis of $BaZrO_3$ by a solid-state reaction technique using nitrate precursors. Materials Research Bulletin. 2002; 37(1): 85-97. doi: 10.1016/S0025-5408(01)00801-7
62. Li Z, Xie Y, Gao J, et al. The promotional effect of multiple active sites on Fe-based oxygen reduction electrocatalysts for a zinc–air battery. Journal of Materials Chemistry A. 2023; 11(48): 26573-26579. doi: 10.1039/d3ta03926a
63. Amdouni W, Otoničar M, Gemeiner P, et al. A General Synthetic Route to High-Quality Perovskite Oxide Nanoparticles and Their Enhanced Solar Photocatalytic Activity. Angewandte Chemie. 2023; 135(7). doi: 10.1002/ange.202215700
64. Zhang X, Li Z, Pei W, et al. Crystal-Phase-Mediated Restructuring of Pt on TiO_2 with Tunable Reactivity: Redispersion versus Reshaping. ACS Catalysis. 2022; 12(6): 3634-3643. doi: 10.1021/acscatal.1c05695
65. Cao D, Luo C, Luo T, et al. Dry reforming of methane by La_2NiO_4 perovskite oxide, part I: Preparation and characterization of the samples. Fuel Processing Technology. 2023; 247: 107765. doi: 10.1016/j.fuproc.2023.107765
66. Shi Q, Zhang X, Li Z, et al. Plasmonic Au Nanoparticle of a Au/TiO_2–C_3N_4 Heterojunction Boosts up Photooxidation of Benzyl Alcohol Using LED Light. ACS Applied Materials & Interfaces. 2023; 15(25): 30161-30169. doi: 10.1021/acsami.3c03451
67. Busari FK, Babar ZUD, Raza A, et al. Unlocking new frontiers: Boosting up electrochemical catalysis with metal clusters and single-atoms. Sustainable Materials and Technologies. 2024; 40: e00958. doi: 10.1016/j.susmat.2024.e00958
68. Shi H, Shi Q, Gu X, et al. Integrating the 2D/2D heterostructure of the MXene monolayer and BiOBr nano-sheets for superior photo-catalysis. Journal of Colloid and Interface Science. 2024; 673: 527-536. doi: 10.1016/j.jcis.2024.06.064
69. Wang M, Fan S, Li X, et al. Construction of Monoatomic-Modified Defective $Ti^{4+}_{\alpha}Ti^{3+}_{1-\alpha}O_{2-\delta}$ Nanofibers for Photocatalytic Oxidation of HMF to Valuable Chemicals. ACS Applied Materials & Interfaces. 2024; 16(5): 5735-5744. doi: 10.1021/acsami.3c14110
70. Yang Y, Yin W, Wu S, et al. Perovskite-Type LaSrMnO Electrocatalyst with Uniform Porous Structure for an Efficient Li–O_2 Battery Cathode. ACS Nano. 2015; 10(1): 1240-1248. doi: 10.1021/acsnano.5b06592
71. Liu R, Liang F, Zhou W, et al. Calcium-doped lanthanum nickelate layered perovskite and nickel oxide nano-hybrid for highly efficient water oxidation. Nano Energy. 2015; 12: 115-122. doi: 10.1016/j.nanoen.2014.12.025
72. Chen CF, King G, Dickerson RM, et al. Oxygen-deficient $BaTiO_{3-x}$ perovskite as an efficient bifunctional oxygen electrocatalyst. Nano Energy. 2015; 13: 423-432. doi: 10.1016/j.nanoen.2015.03.005
73. Han X, Hu Y, Yang J, et al. Porous perovskite $CaMnO_3$ as an electrocatalyst for rechargeable Li–O_2 batteries. Chem Commun. 2014; 50(12): 1497-1499. doi: 10.1039/c3cc48207c
74. Zhao Y, Xu L, Mai L, et al. Hierarchical mesoporous perovskite $La_{0.5}Sr_{0.5}CoO_{2.91}$ nanowires with ultrahigh capacity for Li-air batteries. Proceedings of the National Academy of Sciences. 2012; 109(48): 19569-19574. doi: 10.1073/pnas.1210315109
75. Jin C, Cao X, Zhang L, et al. Preparation and electrochemical properties of urchin-like $La_{0.8}Sr_{0.2}MnO_3$ perovskite oxide as a bifunctional catalyst for oxygen reduction and oxygen evolution reaction. Journal of Power Sources. 2013; 241: 225-230. doi: 10.1016/j.jpowsour.2013.04.116

76. Bai S, Zhang N, Gao C, et al. Defect engineering in photocatalytic materials. Nano Energy. 2018; 53: 296-336. doi: 10.1016/j.nanoen.2018.08.058
77. Guo H, Wan S, Wang Y, et al. Enhanced photocatalytic CO_2 reduction over direct Z-scheme $NiTiO_3$/g-C_3N_4 nanocomposite promoted by efficient interfacial charge transfer. Chemical Engineering Journal. 2021; 412: 128646. doi: 10.1016/j.cej.2021.128646
78. Lv M, Sun X, Wei S, et al. Ultrathin Lanthanum Tantalate Perovskite Nanosheets Modified by Nitrogen Doping for Efficient Photocatalytic Water Splitting. ACS Nano. 2017; 11(11): 11441-11448. doi: 10.1021/acsnano.7b06131
79. Black AP, Suzuki H, Higashi M, et al. New rare earth hafnium oxynitride perovskites with photocatalytic activity in water oxidation and reduction. Chemical Communications. 2018; 54(12): 1525-1528. doi: 10.1039/c7cc08965a
80. Grabowska E, Selected perovskite oxides: Characterization, preparation and photocatalytic properties—A review. Applied Catalysis B: Environmental, 2016; 186: 97–126. doi: 10.1016/j.apcatb.2015.12.035
81. Chen F, Ma T, Zhang T, et al. Atomic-level charge separation strategies in semiconductor-based photocatalysts. Advanced Materials. 2021; 33(10): 2005256. doi: 10.1002/adma.202005256
82. Low J, Yu J, Jaroniec M, et al. Heterojunction Photocatalysts. Advanced Materials. 2017; 29(20). doi: 10.1002/adma.201601694
83. He X, Kai T, Ding P. Heterojunction photocatalysts for degradation of the tetracycline antibiotic: A review. Environmental Chemistry Letters. 2021; 19(6): 4563-4601. doi: 10.1007/s10311-021-01295-8
84. Li X, Yu Z, Shao L, et al. A novel strategy to construct a visible-light-driven Z-scheme (ZnAl-LDH with active phase/g-C_3N_4) heterojunction catalyst via polydopamine bridge (a similar “bridge” structure). Journal of Hazardous Materials. 2020; 386: 121650. doi: 10.1016/j.jhazmat.2019.121650
85. Barkaoui S, Wang Y, Zhang Y, et al. Critical role of NiO support morphology for high activity of Au/NiO nanocatalysts in CO oxidation. iScience. 2024; 27(7): 110255. doi: 10.1016/j.isci.2024.110255
86. Zhao J, Li X, Zhang M, et al. Enhancing the catalytic performance of Co–N–C derived from ZIF-67 by mesoporous silica encapsulation for chemoselective hydrogenation of furfural. Nanoscale. 2023; 15(9): 4612-4619. doi: 10.1039/d2nr05831f
87. Moniz SJA, Shevlin SA, Martin DJ, et al. Visible-light driven heterojunction photocatalysts for water splitting – A critical review. Energy & Environmental Science. 2015; 8(3): 731-759. doi: 10.1039/c4ee03271c
88. Su J, Li G, Li X, et al. 2D/2D Heterojunctions for Catalysis. Advanced Science. 2019; 6(7). doi: 10.1002/advs.201801702
89. Rhimi B, Wang C, Bahnemann DW. Latest progress in g-C_3N_4 based heterojunctions for hydrogen production via photocatalytic water splitting: a mini review. Journal of Physics: Energy. 2020; 2(4): 042003. doi: 10.1088/2515-7655/abb782
90. Lu L, Wu B, Shi W, et al. Metal–organic framework-derived heterojunctions as nanocatalysts for photocatalytic hydrogen production. Inorganic Chemistry Frontiers. 2019; 6(12): 3456-3467. doi: 10.1039/c9qi00964g
91. Afroz K, Moniruddin M, Bakranov N, et al. A heterojunction strategy to improve the visible light sensitive water splitting performance of photocatalytic materials. Journal of Materials Chemistry A. 2018; 6(44): 21696-21718. doi: 10.1039/c8ta04165b
92. Khan MS, Zhang F, Osada M, et al. Graphitic Carbon Nitride-Based Low-Dimensional Heterostructures for Photocatalytic Applications. Solar RRL. 2019; 4(8). doi: 10.1002/solr.201900435
93. He M, Sun K, Suryawanshi MP, et al. Interface engineering of p-n heterojunction for kesterite photovoltaics: A progress review. Journal of Energy Chemistry. 2021; 60: 1-8. doi: 10.1016/j.jechem.2020.12.019
94. Liao X, Li TT, Ren HT, et al. Enhanced photocatalytic performance through the ferroelectric synergistic effect of p-n heterojunction $BiFeO_3$/TiO_2 under visible-light irradiation. Ceramics International. 2021; 47(8): 10786-10795. doi: 10.1016/j.ceramint.2020.12.195
95. Paramanik L, Reddy KH, Sultana S, et al. Architecture of Biperovskite-Based $LaCrO_3$/$PbTiO_3$ p–n Heterojunction with a Strong Interface for Enhanced Charge Anti-recombination Process and Visible Light-Induced Photocatalytic Reactions. Inorganic Chemistry. 2018; 57(24): 15133-15148. doi: 10.1021/acs.inorgchem.8b02364
96. Li S, Hu S, Xu K, et al. Construction of fiber-shaped silver oxide/tantalum nitride p-n heterojunctions as highly efficient visible-light-driven photocatalysts. Journal of Colloid and Interface Science. 2017; 504: 561-569. doi: 10.1016/j.jcis.2017.06.018

97. Heng H, Gan Q, Meng P, et al. The visible-light-driven type III heterojunction $H_3PW_{12}O_{40}/TiO_2$-In_2S_3: A photocatalysis composite with enhanced photocatalytic activity. Journal of Alloys and Compounds. 2017; 696: 51-59. doi: 10.1016/j.jallcom.2016.11.116
98. Ani IJ, Akpan UG, Olutoye MA, et al. Photocatalytic degradation of pollutants in petroleum refinery wastewater by TiO_2- and ZnO-based photocatalysts: Recent development. Journal of Cleaner Production. 2018; 205: 930-954. doi: 10.1016/j.jclepro.2018.08.189
99. Fu J, Yu J, Jiang C, et al. g-C_3N_4-Based Heterostructured Photocatalysts. Advanced Energy Materials. 2017; 8(3). doi: 10.1002/aenm.201701503
100. Chen C, Zhou J, Geng J, et al. Perovskite $LaNiO_3/TiO_2$ step-scheme heterojunction with enhanced photocatalytic activity. Applied Surface Science. 2020; 503: 144287. doi: 10.1016/j.apsusc.2019.144287
101. Fan H, Zhou H, Li W, et al. Facile fabrication of 2D/2D step-scheme $In_2S_3/Bi_2O_2CO_3$ heterojunction towards enhanced photocatalytic activity. Applied Surface Science. 2020; 504: 144351. doi: 10.1016/j.apsusc.2019.144351
102. Li X, Xiong J, Gao X, et al. Novel BP/BiOBr S-scheme nano-heterojunction for enhanced visible-light photocatalytic tetracycline removal and oxygen evolution activity. Journal of Hazardous Materials. 2020; 387: 121690. doi: 10.1016/j.jhazmat.2019.121690
103. Wang R, Shen J, Zhang W, et al. Build-in electric field induced step-scheme $TiO_2/W_{18}O_{49}$ heterojunction for enhanced photocatalytic activity under visible-light irradiation. Ceramics International. 2020; 46(1): 23-30. doi: 10.1016/j.ceramint.2019.08.226
104. He F, Meng A, Cheng B, et al. Enhanced photocatalytic H_2-production activity of WO_3/TiO_2 step-scheme heterojunction by graphene modification. Chinese Journal of Catalysis. 2020; 41(1): 9-20. doi: 10.1016/S1872-2067(19)63382-6
105. He X, Wang A, Wu P, et al. Photocatalytic degradation of microcystin-LR by modified TiO_2 photocatalysis: A review. Science of The Total Environment. 2020; 743: 140694. doi: 10.1016/j.scitotenv.2020.140694
106. Guo H, Yi S, Yang S, et al. Structural symmetry impressing carrier dynamics of halide Perovskite. Advanced Functional Materials. 2023; 33(17): 2214180. doi: 10.1002/adfm.202214180
107. Liang L, Lei F, Gao S, et al. Single Unit Cell Bismuth Tungstate Layers Realizing Robust Solar CO_2 Reduction to Methanol. Angewandte Chemie International Edition. 2015; 54(47): 13971-13974. doi: 10.1002/anie.201506966
108. Cao S, Shen B, Tong T, et al. 2D/2D Heterojunction of Ultrathin MXene/Bi_2WO_6 Nanosheets for Improved Photocatalytic CO_2 Reduction. Advanced Functional Materials. 2018; 28(21). doi: 10.1002/adfm.201800136
109. Kong XY, Lee WQ, Mohamed AR, et al. Effective steering of charge flow through synergistic inducing oxygen vacancy defects and p-n heterojunctions in 2D/2D surface-engineered Bi_2WO_6/BiOI cascade: Towards superior photocatalytic CO_2 reduction activity. Chemical Engineering Journal. 2019; 372: 1183-1193. doi: 10.1016/j.cej.2019.05.001
110. Zhang J, Xie Y, Jiang Q, et al. Facile synthesis of cobalt cluster-CoN_x composites: Synergistic effect boosts electrochemical oxygen reduction. Journal of Materials Chemistry A. 2022; 10(32): 16920-16927. doi: 10.1039/d2ta04413g
111. Choi BN, Seo JY, An Z, et al. An in-situ spectroscopic study on the photochemical CO_2 reduction on $CsPbBr_3$ perovskite catalysts embedded in a porous copper scaffold. Chemical Engineering Journal. 2022; 430: 132807. doi: 10.1016/j.cej.2021.132807
112. Xu Q, Wang L, Sheng X, et al. Understanding the synergistic mechanism of single atom Co-modified perovskite oxide for piezo-photocatalytic CO_2 reduction. Applied Catalysis B: Environmental. 2023; 338: 123058. doi: 10.1016/j.apcatb.2023.123058
113. Stolarczyk JK, Bhattacharyya S, Polavarapu L, et al. Challenges and Prospects in Solar Water Splitting and CO_2 Reduction with Inorganic and Hybrid Nanostructures. ACS Catalysis. 2018; 8(4): 3602-3635. doi: 10.1021/acscatal.8b00791
114. Álvarez A, Bansode A, Urakawa A, et al. Challenges in the Greener Production of Formates/Formic Acid, Methanol, and DME by Heterogeneously Catalyzed CO_2 Hydrogenation Processes. Chemical Reviews. 2017; 117(14): 9804-9838. doi: 10.1021/acs.chemrev.6b00816
115. Xu L, Ha MN, Guo Q, et al. Photothermal catalytic activity of combustion synthesized $LaCo_xFe_{1-x}O_3$ ($0 \leq x \leq 1$) perovskite for CO_2 reduction with H_2O to CH_4 and CH_3OH. RSC Adv. 2017; 7(73): 45949-45959. doi: 10.1039/c7ra04879c
116. Jiao X, Chen Z, Li X, et al. Defect-Mediated Electron–Hole Separation in One-Unit-Cell $ZnIn_2S_4$ Layers for Boosted Solar-Driven CO_2 Reduction. Journal of the American Chemical Society. 2017; 139(22): 7586-7594. doi: 10.1021/jacs.7b02290
117. Xie K, Umezawa N, Zhang N, et al. Self-doped $SrTiO_{3-\delta}$ photocatalyst with enhanced activity for artificial photosynthesis under visible light. Energy & Environmental Science. 2011; 4(10): 4211. doi: 10.1039/c1ee01594j

118. Xu F, Meng K, Cheng B, et al. Unique S-scheme heterojunctions in self-assembled TiO_2/$CsPbBr_3$ hybrids for CO_2 photoreduction. Nature Communications. 2020; 11(1). doi: 10.1038/s41467-020-18350-7
119. Sun Z, Wang H, Wu Z, et al. g-C_3N_4 based composite photocatalysts for photocatalytic CO_2 reduction. Catalysis Today. 2018; 300: 160-172. doi: 10.1016/j.cattod.2017.05.033
120. Li K, Handoko AD, Khraisheh M, et al. Photocatalytic reduction of CO_2 and protons using water as an electron donor over potassium tantalate nanoflakes. Nanoscale. 2014; 6(16): 9767. doi: 10.1039/c4nr01490a
121. Yoshida H, Zhang L, Sato M, et al. Calcium titanate photocatalyst prepared by a flux method for reduction of carbon dioxide with water. Catalysis Today. 2015; 251: 132-139. doi: 10.1016/j.cattod.2014.10.039
122. Wu X, Wang C, Wei Y, et al. Multifunctional photocatalysts of Pt-decorated 3DOM perovskite-type $SrTiO_3$ with enhanced CO_2 adsorption and photoelectron enrichment for selective CO_2 reduction with H_2O to CH_4. Journal of Catalysis. 2019; 377: 309-321. doi: 10.1016/j.jcat.2019.07.037
123. Teramura K, Okuoka S ichi, Tsuneoka H, et al. Photocatalytic reduction of CO_2 using H_2 as reductant over $ATaO_3$ photocatalysts (A = Li, Na, K). Applied Catalysis B: Environmental. 2010; 96(3-4): 565-568. doi: 10.1016/j.apcatb.2010.03.021
124. Cheng YH, Nguyen VH, Chan HY, et al. Photo-enhanced hydrogenation of CO_2 to mimic photosynthesis by CO co-feed in a novel twin reactor. Applied Energy. 2015; 147: 318-324. doi: 10.1016/j.apenergy.2015.02.085
125. Shi H, Zhang C, Zhou C, et al. Conversion of CO_2 into renewable fuel over Pt–g-C_3N_4/$KNbO_3$ composite photocatalyst. RSC Advances. 2015; 5(113): 93615-93622. doi: 10.1039/c5ra16870h
126. Do JY, Im Y, Kwak BS, et al. Preparation of basalt fiber@perovskite $PbTiO_3$ core–shell composites and their effects on CH4 production from CO_2 photoreduction. Ceramics International. 2016; 42(5): 5942-5951. doi: 10.1016/j.ceramint.2015.12.142
127. Chen X, Wang J, Huang C, et al. Barium zirconate: a new photocatalyst for converting CO_2 into hydrocarbons under UV irradiation. Catalysis Science & Technology. 2015; 5(3): 1758-1763. doi: 10.1039/c4cy01201a
128. Jia L, Li J, Fang W, et al. Visible-light-induced photocatalyst based on C-doped $LaCoO_3$ synthesized by novel microorganism chelate method. Catalysis Communications. 2009; 10(8): 1230-1234. doi: 10.1016/j.catcom.2009.01.025
129. Fresno F, Jana P, Reñones P, et al. CO_2 reduction over $NaNbO_3$ and $NaTaO_3$ perovskite photocatalysts. Photochemical & Photobiological Sciences. 2017; 16(1): 17-23. doi: 10.1039/c6pp00235h
130. Wang J, Huang C, Chen X, et al. Photocatalytic CO_2 reduction of $BaCeO_3$ with 4f configuration electrons. Applied Surface Science. 2015; 358: 463-467. doi: 10.1016/j.apsusc.2015.08.063
131. Hou J, Cao S, Wu Y, et al. Inorganic Colloidal Perovskite Quantum Dots for Robust Solar CO_2 Reduction. Chemistry – A European Journal. 2017; 23(40): 9481-9485. doi: 10.1002/chem.201702237
132. Zhou H, Li P, Guo J, et al. Artificial photosynthesis on tree trunk derived alkaline tantalates with hierarchical anatomy: towards CO_2 photo-fixation into CO and CH_4. Nanoscale. 2015; 7(1): 113-120. doi: 10.1039/c4nr03019b
133. Wang S, Hou Y, Wang X. Development of a Stable $MnCo_2O_4$ Cocatalyst for Photocatalytic CO_2 Reduction with Visible Light. ACS Applied Materials & Interfaces. 2015; 7(7): 4327-4335. doi: 10.1021/am508766s
134. Li H, Shang J, Ai Z, et al. Efficient Visible Light Nitrogen Fixation with BiOBr Nanosheets of Oxygen Vacancies on the Exposed {001} Facets. Journal of the American Chemical Society. 2015; 137(19): 6393-6399. doi: 10.1021/jacs.5b03105
135. Hoffman BM, Lukoyanov D, Yang ZY, et al. Mechanism of Nitrogen Fixation by Nitrogenase: The Next Stage. Chemical Reviews. 2014; 114(8): 4041-4062. doi: 10.1021/cr400641x
136. Giddey S, Badwal SPS, Kulkarni A. Review of electrochemical ammonia production technologies and materials. International Journal of Hydrogen Energy. 2013; 38(34): 14576-14594. doi: 10.1016/j.ijhydene.2013.09.054
137. Yang J, Guo Y, Jiang R, et al. High-Efficiency “Working-in-Tandem” Nitrogen Photofixation Achieved by Assembling Plasmonic Gold Nanocrystals on Ultrathin Titania Nanosheets. Journal of the American Chemical Society. 2018; 140(27): 8497-8508. doi: 10.1021/jacs.8b03537
138. Li Q, Bai X, Luo J, et al. Fe doped $SrWO_4$ with tunable band structure for photocatalytic nitrogen fixation. Nanotechnology. 2020; 31(37): 375402. doi: 10.1088/1361-6528/ab9863
139. Chen X, Li N, Kong Z, et al. Photocatalytic fixation of nitrogen to ammonia: State-of-the-art advancements and future prospects. Materials Horizons. 2018; 5(1): 9-27. doi: 10.1039/c7mh00557a
140. Shipman MA, Symes MD. Recent progress towards the electrosynthesis of ammonia from sustainable resources. Catalysis Today. 2017; 286: 57-68. doi: 10.1016/j.cattod.2016.05.008

141. Azofra LM, Li N, MacFarlane DR, et al. Promising prospects for 2D d^2–$d^4M_3C_2$ transition metal carbides (MXenes) in N_2 capture and conversion into ammonia. Energy & Environmental Science. 2016; 9(8): 2545-2549. doi: 10.1039/c6ee01800a
142. Zhou S, Zhang C, Liu J, et al. Formation of an oriented Bi_2WO_6 photocatalyst induced by in situ Bi reduction and its use for efficient nitrogen fixation. Catalysis Science & Technology. 2019; 9(20): 5562-5566. doi: 10.1039/c9cy00972h
143. Xing P, Wu S, Chen Y, et al. New Application and Excellent Performance of Ag/$KNbO_3$ Nanocomposite in Photocatalytic NH_3 Synthesis. ACS Sustainable Chemistry & Engineering. Published online June 26, 2019. doi: 10.1021/acssuschemeng.9b01938
144. Tao R, Li X, Li X, et al. TiO_2/$SrTiO_3$/g-C_3N_4 ternary heterojunction nanofibers: Gradient energy band, cascade charge transfer, enhanced photocatalytic hydrogen evolution, and nitrogen fixation. Nanoscale. 2020; 12(15): 8320-8329. doi: 10.1039/d0nr00219d
145. Mansingh S, Sultana S, Acharya R, et al. Correction to Efficient Photon Conversion via Double Charge Dynamics CeO_2–$BiFeO_3$ p–n Heterojunction Photocatalyst Promising toward N_2 Fixation and Phenol–Cr(VI) Detoxification. Inorganic Chemistry. 2020; 59(9): 6646-6646. doi: 10.1021/acs.inorgchem.0c00981
146. Mansingh S, Sultana S, Acharya R, et al. Efficient Photon Conversion via Double Charge Dynamics CeO_2–$BiFeO_3$ p–n Heterojunction Photocatalyst Promising toward N_2 Fixation and Phenol–Cr(VI) Detoxification. Inorganic Chemistry. 2020; 59(6): 3856-3873. doi: 10.1021/acs.inorgchem.9b03526
147. Zhang H, Li X, Su H, et al. Sol–gel synthesis of upconversion perovskite/attapulgite heterostructures for photocatalytic fixation of nitrogen. Journal of Sol-Gel Science and Technology. 2019; 92(1): 154-162. doi: 10.1007/s10971-019-05071-7
148. Shi L, Ren X, Wang Q, et al. Stabilizing Atomically Dispersed Catalytic Sites on Tellurium Nanosheets with Strong Metal–Support Interaction Boosts Photocatalysis. Small. 2020; 16(35). doi: 10.1002/smll.202002356
149. Qiao B, Wang A, Yang X, et al. Single-atom catalysis of CO oxidation using Pt_1/FeO_x. Nature Chemistry. 2011; 3(8): 634-641. doi: 10.1038/nchem.1095
150. Qin Z, Li Z, Sharma S, et al. Self-Assembly of Silver Clusters into One- and Two-Dimensional Structures and Highly Selective Methanol Sensing. Research. 2022; 2022. doi: 10.34133/research.0018
151. Liu X, Zhang Y, Li Z, et al. Surface ligand engineering on the optical properties of atomically precise AuAg nanoclusters. Chinese Journal of Structural Chemistry. 2023; 42(9): 100154. doi: 10.1016/j.cjsc.2023.100154
152. Cao Y, Su Y, Xu L, et al. Oxygen vacancy-rich amorphous FeNi hydroxide nanoclusters as an efficient electrocatalyst for water oxidation. Journal of Energy Chemistry. 2022; 71: 167-173. doi: 10.1016/j.jechem.2022.03.044
153. Huang G, Lin G, Niu Q, et al. Covalent triazine-based frameworks confining cobalt single atoms for photocatalytic CO_2 reduction and hydrogen production. Journal of Materials Science & Technology. 2022; 116: 41-49. doi: 10.1016/j.jmst.2021.11.035
154. Gao C, Chen S, Wang Y, et al. Heterogeneous Single-Atom Catalyst for Visible-Light-Driven High-Turnover CO_2 Reduction: The Role of Electron Transfer. Advanced Materials. 2018; 30(13). doi: 10.1002/adma.201704624
155. Shi Q, Zhang X, Liu X, et al. In-situ exfoliation and assembly of 2D/2D g-C_3N_4/TiO_2(B) hierarchical microflower: Enhanced photo-oxidation of benzyl alcohol under visible light. Carbon. 2022; 196: 401-409. doi: 10.1016/j.carbon.2022.05.007
156. Jin C, Dai Y, Wei W, et al. Effects of single metal atom (Pt, Pd, Rh and Ru) adsorption on the photocatalytic properties of anatase TiO_2. Applied Surface Science. 2017; 426: 639-646. doi: 10.1016/j.apsusc.2017.07.065
157. Yang C, Zhao ZY, Wei HT, et al. DFT calculations for single-atom confinement effects of noble metals on monolayer g-C_3N_4 for photocatalytic applications. RSC Advances. 2021; 11(7): 4276-4285. doi: 10.1039/d0ra09815a
158. Guo Y, Xia M, Zhang M, et al. A strategy for enhancing the photoactivity of g-C_3N_4-based single-atom catalysts via sulphur doping: A theoretical study. Physical Chemistry Chemical Physics. 2021; 23(11): 6632-6640. doi: 10.1039/d1cp00192b
159. Xin J, Li F, Li Z, et al. Controlling the band structure and photocatalytic performance of single atom Ag/C_3N_4 catalysts by variation of silver concentration. Inorganic Chemistry Frontiers. 2022; 9(2): 302-309. doi: 10.1039/d1qi01138c
160. Xiong X, Mao C, Yang Z, et al. Photocatalytic CO_2 Reduction to CO over Ni Single Atoms Supported on Defect-Rich Zirconia. Advanced Energy Materials. 2020; 10(46). doi: 10.1002/aenm.202002928
161. Liu Y, Xu L, Zhang N, et al. A promoted charge separation/transfer and surface plasmon resonance effect synergistically enhanced photocatalytic performance in Cu nanoparticles and single-atom Cu supported attapulgite/polymer carbon nitride photocatalyst. Materials Today Chemistry. 2022; 26: 101250. doi: 10.1016/j.mtchem.2022.101250
162. Gao Y, Wu J, Wang G, et al. Construction of the charge transfer channels for enhanced photocatalytic CO_2 reduction reaction. Chemical Engineering Science. 2022; 264: 118166. doi: 10.1016/j.ces.2022.118166

163. Yan B, He Y, Yang G. Electronic structure regulation of cobalt oxide clusters for promoting photocatalytic hydrogen evolution. Journal of Materials Chemistry A. 2022; 10(4): 1899-1908. doi: 10.1039/d1ta08279e
164. Feng Y, Wang C, Cui P, et al. Ultrahigh Photocatalytic CO_2 Reduction Efficiency and Selectivity Manipulation by Single-Tungsten-Atom Oxide at the Atomic Step of TiO_2. Advanced Materials. 2022; 34(17). doi: 10.1002/adma.202109074
165. Halmann M. Photoelectrochemical reduction of aqueous carbon dioxide on p-type gallium phosphide in liquid junction solar cells. Nature. 1978; 275(5676): 115-116. doi: 10.1038/275115a0
166. Gao G, Jiao Y, Waclawik ER, et al. Single Atom (Pd/Pt) Supported on Graphitic Carbon Nitride as an Efficient Photocatalyst for Visible-Light Reduction of Carbon Dioxide. Journal of the American Chemical Society. 2016; 138(19): 6292-6297. doi: 10.1021/jacs.6b02692
167. Zhao C, Liu J, Li B, et al. Multiscale Construction of Bifunctional Electrocatalysts for Long-Lifespan Rechargeable Zinc–Air Batteries. Advanced Functional Materials. 2020; 30(36). doi: 10.1002/adfm.202003619
168. Wu S, He C, Wang L, et al. High-efficiency electron tandem flow mode on carbon nitride/titanium dioxide heterojunction for visible light nitrogen photofixation. Chemical Engineering Journal. 2022; 443: 136425. doi: 10.1016/j.cej.2022.136425
169. Wang J, Liu W, Luo G, et al. Synergistic effect of well-defined dual sites boosting the oxygen reduction reaction. Energy & Environmental Science. 2018; 11(12): 3375-3379. doi: 10.1039/c8ee02656d
170. Yin H, Chen Z, Peng Y, et al. Dual Active Centers Bridged by Oxygen Vacancies of Ruthenium Single-Atom Hybrids Supported on Molybdenum Oxide for Photocatalytic Ammonia Synthesis. Angewandte Chemie International Edition. 2022; 61(14). doi: 10.1002/anie.202114242
171. Li J, Liu P, Tang Y, et al. Single-Atom Pt–N_3 Sites on the Stable Covalent Triazine Framework Nanosheets for Photocatalytic N_2 Fixation. ACS Catalysis. 2020; 10(4): 2431-2442. doi: 10.1021/acscatal.9b04925